EPRI

REV 2 DRAFT

Methodology for Estimating Tidal Current Energy Resources and Power Production by Tidal In-Stream Energy Conversion (TISEC) Devices

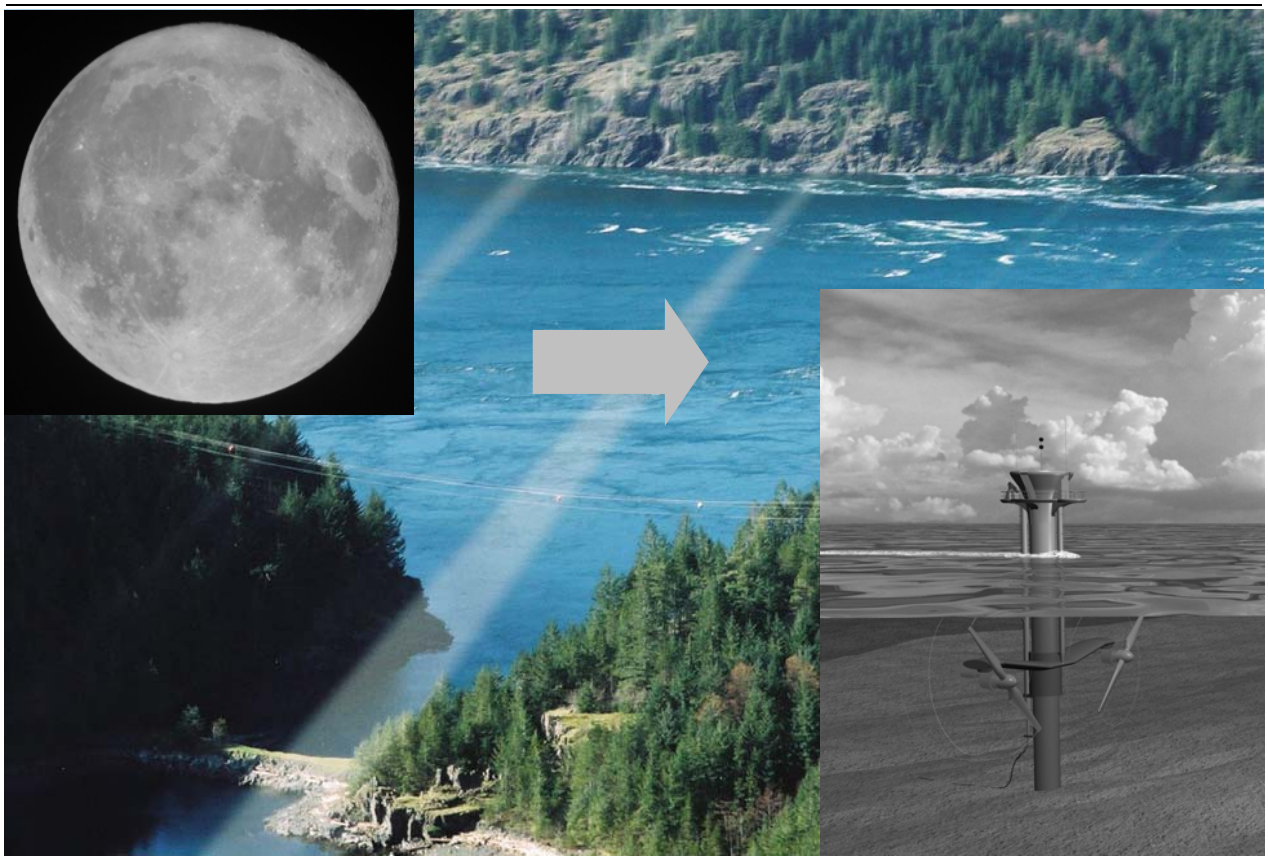

Project: EPRI North American Tidal In Stream Power Feasibility Demonstration Project
Phase: 1 – Project Definition Study
Report: EPRI – TP – 001 NA Rev 2
Authors: George Hagerman and Brian Polagye
Coauthors Roger Bedard and Mirko Previsic
Date: June 14, 2006

DISCLAIMER OF WARRANTIES AND LIMITATION OF LIABILITIES

This document was prepared by the organizations named below as an account of work sponsored or cosponsored by the Electric Power Research Institute Inc. (EPRI). Neither EPRI, any member of EPRI, any cosponsor, the organization (s) below, nor any person acting on behalf of any of them:

(A) Makes any warranty or representation whatsoever, express or implied, (I) with respect to the use of any information, apparatus, method, process or similar item disclosed in this document, including merchantability and fitness for a particular purpose, or (II) that such use does not infringe on or interfere with privately owned rights, including any parties intellectual property, or (III) that this document is suitable to any particular user's circumstance; or

(B) Assumes responsibility for any damages or other liability whatsoever (including any consequential damages, even if EPRI or any EPRI representative has been advised of the possibility of such damages) resulting for your selection or use of this document or any other information, apparatus, method, process or similar item disclosed in this document.

Organization(s) that prepared this document

Electric Power Research Institute (Roger Bedard)

Virginia Polytechnic Institute and State University (George Hagerman)

University of Washington (Brian Polagye)

Mirko Previsic Consulting (Mirko Previsic)

Table of Contents

1. Introduction and Overview

1.1. Introduction

1.2. Background

1.3. Tidal Energy Fundamentals

1.4. Overview of Tidal Stream Energy Conversion Methodology

2. Tidal Current Data Sources

2.1. United States
- 2.1.1. Tidal Current Predictions by the National Ocean Survey (NOS)
- 2.1.2. Tidal Current Table Formats
- 2.1.3. U.S. Geographical Coverage
- 2.1.4. Characteristics of Primary Tidal Current Reference Stations
- 2.1.5. Example Tidal Current Table Data
- 2.1.6. Tidal Current Prediction Software

2.2. Canada
- 2.2.1. Canadian Hydrographic Service (CHS) Publications
- 2.2.2. Department of Fisheries and Oceans (DFO) Software – *WebTide*

3. Tidal Stream Resource Methodology for Site Survey Reports

3.1. Site Screening

3.2. Mean Annual Power Density
- 3.2.1. Surface Current Velocities
- 3.2.2. Accounting for Velocity Variability with Depth
- 3.2.3. Accounting for Velocity Variability across Channel

3.3. Channel Cross-Sectional Area

3.4. Total Available Resource

3.5. Extractable Resource

4. Tidal Stream Power Production Methodology for Design Reports

4.1. Surface Current Velocity Distribution
- 4.1.1. Sinusoidal Fit of Velocity Time History to Tidal Current Table Data
- 4.1.2. Extrapolation of Velocity Time History to a Different Channel Section
- 4.1.3. *WebTide* Velocity Time History for Head Harbour Passage, NB
- 4.1.4. *WebTide* Velocity Time History for Minas Passage, NS

4.2. Turbine Hub-Height Current Velocity Distribution

4.3. Electric Power Output

4.4. Annual Energy Production

4.5. Spacing of Turbines within Project

4.6. Maximum Project Size
- 4.6.1. Influence of Tidal Range on Physical Resource Estimates
- 4.6.2. Energy Extraction Constraints
- 4.6.3. Turbine Spacing and Physical Placement Constraints
- 4.6.4. Number of Homes Powered

5. References

Appendix A – Fluid Flow Power Theory: Wind and Tidal Stream Comparisons

Appendix B – Creation of Digitized Channel Cross-Sections from Soundings Data

1. Introduction and Overview

1.1. Introduction

The EPRI North American Tidal In Stream Energy Conversion (TISEC) Power Project will demonstrate the feasibility of tidal current power to provide efficient, reliable, environmentally friendly and cost-effective electrical energy and to create a push towards the development of a sustainable commercial market for this technology. This project is being conducted by a team consisting of the Electric Power Research Institute (EPRI), EPRIsolutions, a subsidiary of EPRI, Virginia Tech, the University of Washington, Mirko Previsic (private consultant), Devine Tarbell and Associates (TDA) and the Department of Energy's National Renewable Energy Laboratory (NREL), herein referred to as "the Project Team."

EPRI is a non-profit science and technology energy industry collaborative organization that provides a wide range of innovative products and services to more than 700 energy-related organizations in 40 countries and has an annual budget of about $300 million. EPRI's multidisciplinary teams of scientists and engineers draw on a worldwide network of technical and business expertise to help solve today's toughest energy and environmental problems.

1.2. Background

Published data on TISEC energy conversion devices seldom provide sufficient detail to assess the magnitude and accuracy of power production claims. Wind turbine manufacturers routinely publish turbine performance data in the form of curves and/or tables depicting generated power as a function of wind speed (for example, see General Electric 3.6-MW turbine specifications at http://www.gepower.com/prod_serv/products/wind_turbines/en/index.htm, or the Vestas 2-MW turbine specifications at http://www.natwindpower.co.uk/northhoyle/gsv80.pdf), but at this time, tidal stream turbine developers rarely provide similar information on output power as a function of flow speed.

This lack of documentation also makes it difficult to compare the likely performance of different TISEC energy conversion devices in a given tidal stream flow climate, particularly when different underlying assumptions and simulation or model test methods have been used to generate their power production estimates. Finally, without such documentation, it is impossible to establish a "baseline" performance against which industry improvements can be benchmarked.

The purpose of this guideline document is to provide a methodology that will enable the Project Team to estimate the power and energy production of different TISEC devices at various sites with their native tidal stream flow climate.

1.3. Tidal Energy Fundamentals

Tidal power was one of the earliest forms of renewable energy to be used by mankind. As far back as the eighth century, the Spanish, French and British built tidal storage ponds behind dams that were filled by the incoming tide through sluice gates. These gates were closed at high tide and the trapped water directed back to the sea through a water wheel to mill grain. The Eling Tide Mill in the United Kingdom has been producing flour with tidal power for 900 years and still does so today (see http://www.elingtidemill.wanadoo.co.uk/sitem.html for a description).

A few tidal power electrical-generation plants have been built that operate on a similar principal, by building a dam or barrage to impound the water at high tide and then releasing the water through conventional hydroelectric turbine-generators when the difference between the falling ocean level seaward of the dam and the trapped water in the pond behind the dam is sufficiently great to drive the turbines. These include the 240 MW project built in the mid-1960s on the La Rance River estuary in France, a 500 kW project at Kislaya Gubska in Russia (which pioneered float-in-place caisson construction for the dam), and the 20 MW project built in the 1980s at Annapolis Royal, Nova Scotia, pioneering the use of a Straflo rim-driven turbine-generator.

Because of the vast civil engineering works involved in building the dam or barrage, such impoundment projects must be very large in order to be economical, and this has unacceptable environmental impacts, which arrested further development of this technology. Recently, however, submerged tidal current turbines, similar to underwater wind turbines driven by water flow rather than airflow, have reached a level of engineering maturity and near-commercial development that EPRI conceived the TISEC project to further explore their techno-economic feasibility in five states: Alaska (AK), Washington (WA), San Francisco (SF), Massachusetts (MA), Maine (ME), and two provinces: New Brunswick (NB) and Nova Scotia (NS).

The major benefits of tidal power are that it is non-polluting, reliable and predictable. Tidal energy is, however, variable and being driven primarily by the moon rather than the sun, its peak availability is governed by the lunar orbital period of 24 hours and 50 minutes, whereas civilization's peak energy demand is governed by the Earth's rotational period of 24 hours. Thus the peak in tidal power availability is 50 minutes later from one day to the next.

For an energy source to be viable and useful in modern power markets, it does not necessarily need to be constant, but it must be reliable; i.e., a utility provider must be able to predict when the supply will be available and in what quantities so that it can be matched with other generation sources to meet demand. This poses a problem for renewable generation technologies dependent on weather conditions, such as solar, wind and wave, since their variability is stochastic in nature, i.e. a project can experience a few hours of windy or sunny weather, or it can experience a few days of windy or sunny weather. Moreover, daytime solar energy fluxes can be forecast only minutes ahead (due to the vagaries of cloud formation), wind for hours ahead, and ocean waves for days ahead, with decreasing precision as the forecast time is extended. Being dependent on deterministic astronomical forces rather than weather, tidal power is much more predictable than solar, wind or wave power. If the tidal current flow regime at a particular location has been properly studied (i.e. measured for at least 29 days), its variation can be predicted with considerable accuracy over the entire 20- or 30-year life of the project.

Tides are generated by the rotation of the earth within its ocean envelope as shaped by the gravitational fields of the moon and sun. To an observer at a given location on the rotating earth, this causes local sea level to periodically rise and fall according to highly predictable, interacting harmonic cycles, as described below.

The moon's gravitation creates tidal "tractive forces" that create two "bulges" in the earth's ocean envelope: one bulge on the side of the earth facing the moon, and the other bulge on the opposite side of the earth (see Figure 1-1). Rotation of the earth within these "bulges" result in two tides (high water to low water sequence) per day, or semi-diurnal tides, which is the dominant tidal pattern in most of the world's oceans.

Vectors on the earth's surface in the diagram below indicate the difference between the gravitational force the moon exerts at a given point on earth's surface and the force it would exert at the earth's center. These resultant force vectors move water toward the earth-moon orbital plane, creating two bulges on opposite sides of the earth. See http://www.lhup.edu/~dsimanek/scenario/tides.htm for a full explanation.

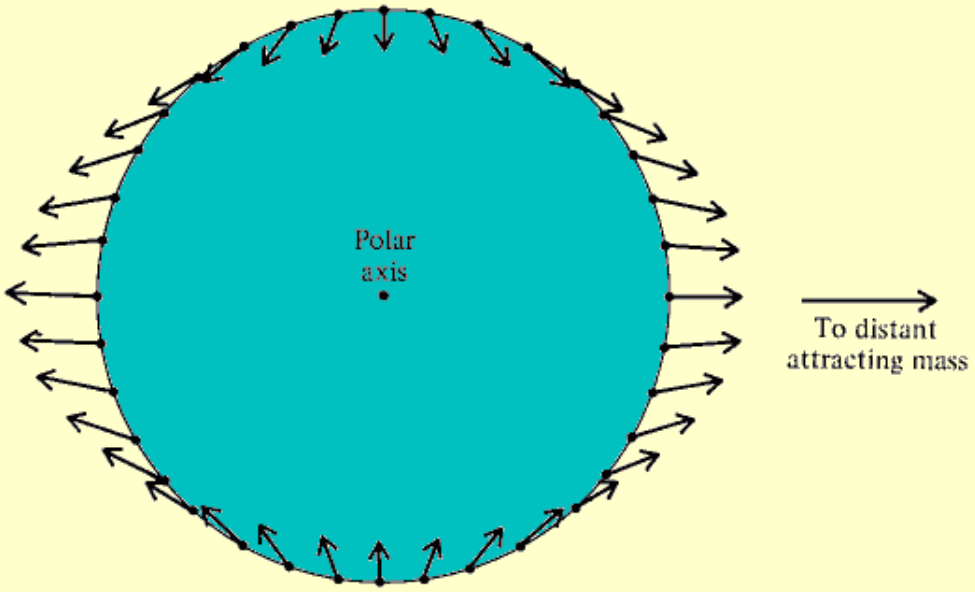

Figure 1-1. Tide-Generating Forces Based on Earth-Moon Interactions

Considering the declination of the moon's orbital plane relative to the earth's axis of rotation complicates the picture somewhat. On a smooth earth without continents or ocean basins, this declination produces semi-diurnal tides (two high tides and two low tides per day) near the equator, and diurnal tides at high latitudes, as shown in Figure 1-2. Mid-latitude locations experience mixed tides, with two tides per day, but with significant diurnal inequality between successive high waters and successive low waters.

This influence changes as the moon's declination progresses from its extreme position over the north tropic to its extreme position over the south tropic, 14 days later. When the moon is over the equator, between these extremes, the diurnal inequality is minimized, which happens twice per tropical month (which is 27.3 days long).

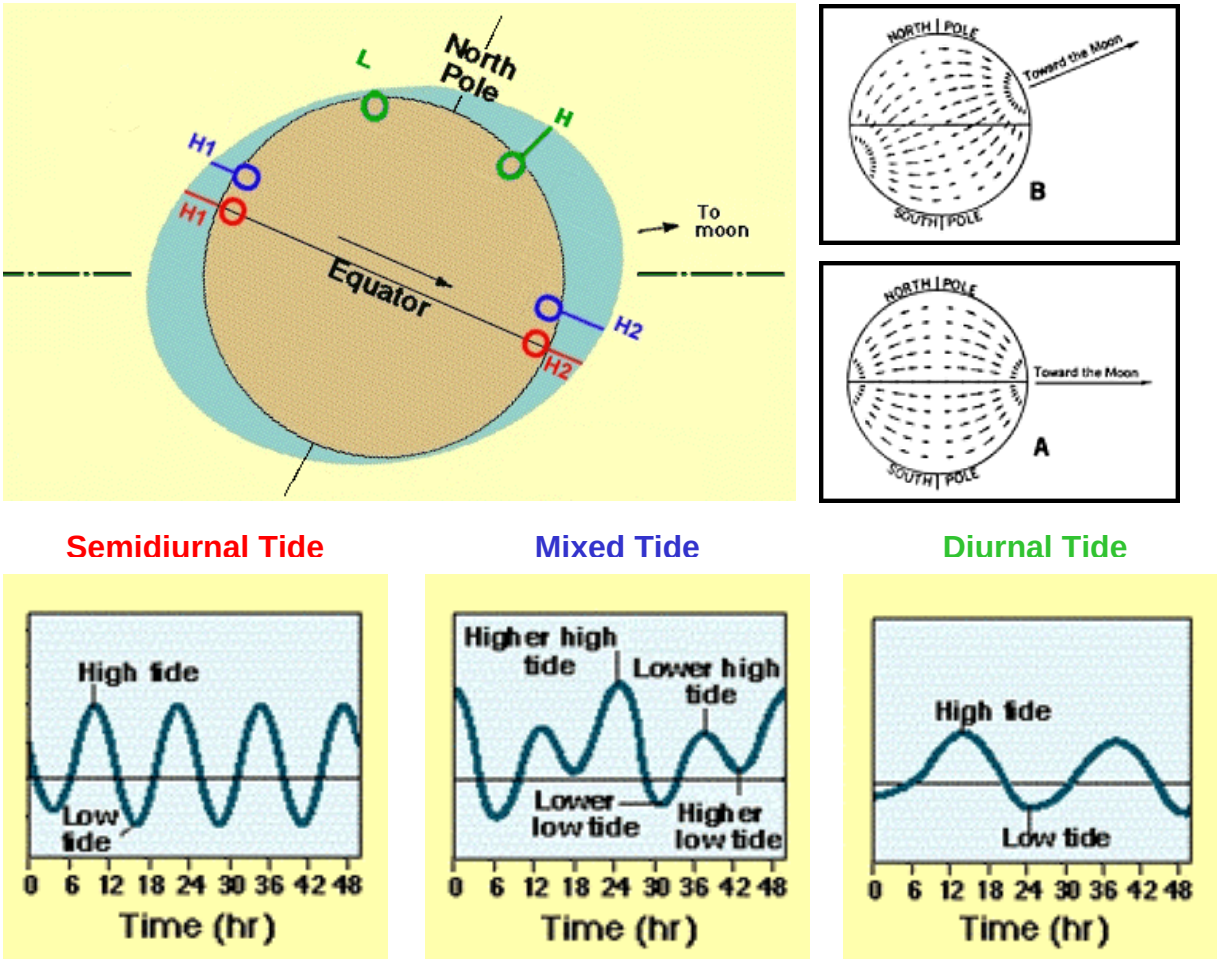

Figure 1-2. Influence of Moon's Declination on Tidal Forces

The tilt of the Moon's orbit combines with the tilt of the Earth's axis of rotation to cause the Moon's declination, as observed from Earth, to vary between ±28.6° (when the two inclinations are additive), and ±18.3° (when the two inclinations oppose each other). These maxima and minima of lunar declination repeat every 18.6 years, the longest-period tidal constituent.

On a non-uniform earth, the tidal bulge is fragmented by continents as it flows into various ocean basins, creating a more complex distribution of predominant tidal types, which is shown in Figure 1-3. Note that this has a significant influence on the capacity factor of tidal in-stream conversion devices, reducing their capacity factor at North American west coast locations with significant diurnal inequality (such as in AK, WA and SF), and increasing their capacity factor at east coast sites that have predominantly semi-diurnal tides (such as MA, ME, NB and NS).

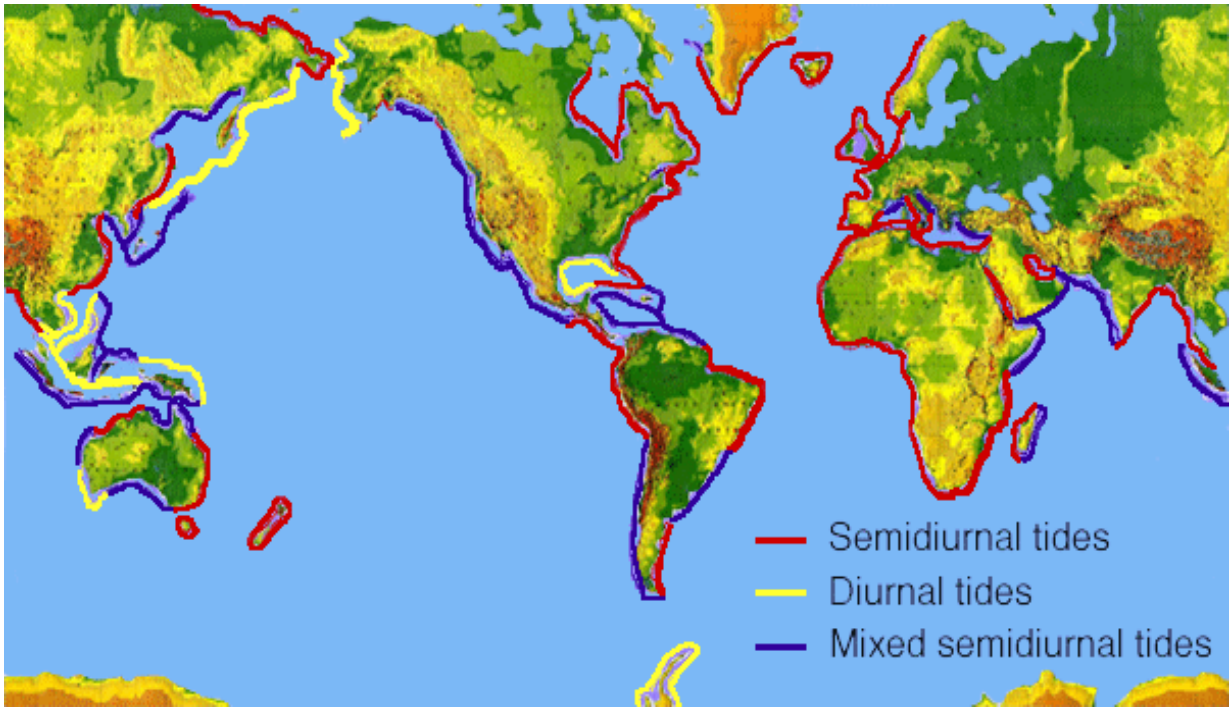

Figure 1-3 Global Distribution of Tidal Regimes

The amplitude of the solar tidal bulges is only 46% as high as the lunar tidal bulges. While the lunar bulges migrate around the Earth once every 27 days; the solar bulges migrate around the Earth once every day. As the lunar bulge moves exactly into and then 90° out of phase with the solar bulge, this gives rise to spring and neap tides, respectively, as illustrated in Figure 1-4.

The combined lunar-solar tidal bulge is predominantly lunar with modifying solar effects on the height of the tide and the direction of the tidal bulge according to the phases of the moon. During the times of new and full moon, when the earth, moon, and sun lie approximately on the same line, the resultant tides are called spring tides, whose ranges are greater than average. Note that "spring" does not refer to the season but is derived from the German word *springen* – "to leap"). Mid-way between spring tides, the moon is at first and third quarters. At those times, the sun's tidal forces act at right angles to the moon's tidal forces, creating lower high tides and higher low tides. The resulting tides are called neap tides, whose ranges are less than average. Spring tidal ranges are typically about twice neap tidal ranges, and their influence on tidal current velocities is substantial, as shown in Figure 1-4.

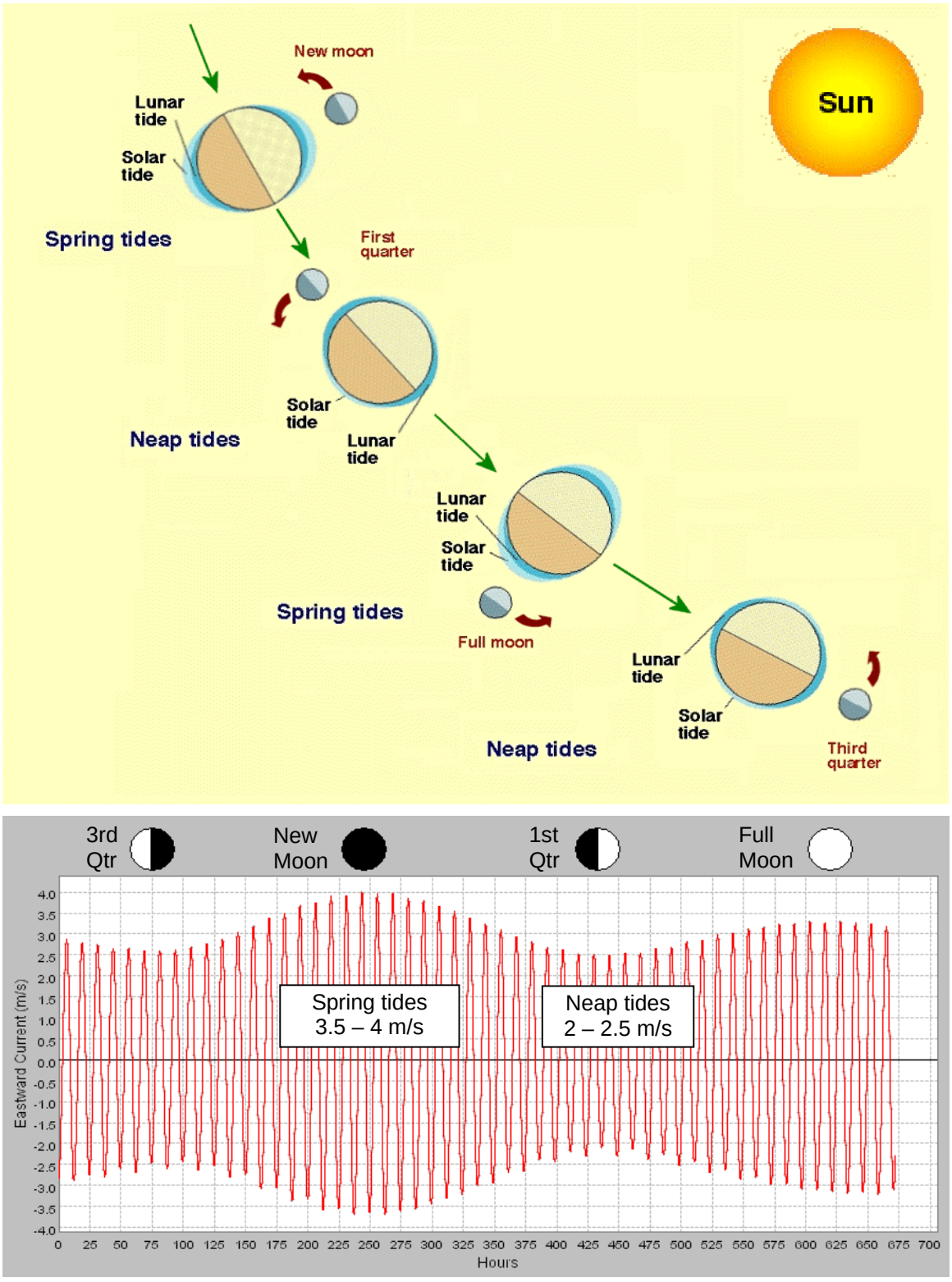

Figure 1-4 Moon Phases Causing Spring and Neap Tides (Tidal current example from off Cape Sharp in Minas Passage, NS)

The combination of the spring to neaps cycle every 14 days results in a variability of tidal range and current speed through the months of the year. There are dozens of other astronomical forcing constituents (harmonic components) of the tide, each with a different period and amplitude. Several of the most significant constituents are shown in Figure 1-5.

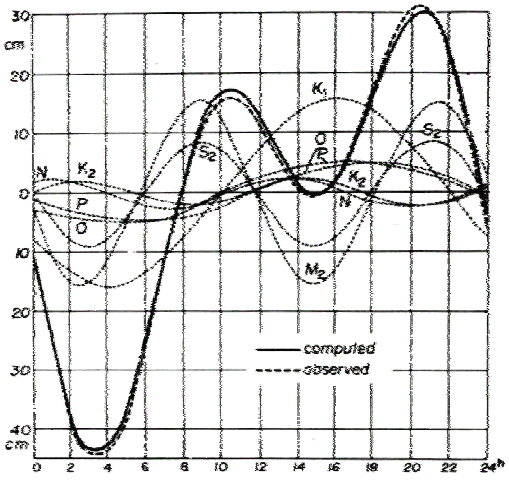

The Most Important of the Tide-generating Constituents (*After* Defant, 1958)

SYMBOL	PERIOD (SOLAR HR)	AMPLITUDE (M_2 = 100)	DESCRIPTION
M_2	12.42	100.0	Main lunar semidiurnal constituent
S_2	12.00	46.6	Main solar semidiurnal constituent
N	12.66	19.1	Lunar constituent due to monthly variation in moon's distance
K_2	11.97	12.7	Solar-lunar constituent due to changes in declination of sun and moon throughout their orbital cycle
K_1	23.93	58.4	Solar-lunar constituent
O	25.82	41.5	Main lunar diurnal constituent
P	24.07	19.3	Main solar diurnal constituent
M_f	327.86	17.2	Moon's fortnightly constituent

Figure 1-5 Typical Phase Relationship Between Tide Level and Tidal Current Speed

The longest period of any tidal constituent is 18.6 years, which is the period between extremes in the lunar declination cycle, as previously described. A measurement record length of 369 days is sufficient to capture the most significant astronomical forcing constituents, however, and even a 29-day record yields enough information to generate a year-long tidal prediction (Reference 1).

The duration of slack water will vary, depending upon location and time of year. In good tidal stream energy conversion sites (average of spring and neap tidal currents speeds in the range of 2 to 3 m/s or 4 to 6 knots), the duration of slack water is typically measured in tens of minutes, and TISEC device developers must account for this short available working time in developing offshore procedures for installing or removing their devices as well as access for inspection, maintenance, and repair, which may involve replacing one device with another so that a device in need of service can be towed to a shoreside support facility.

Tidal current speeds predicted from astronomical harmonic constituents can be modified by wind stress acting for extended periods, which may blow water into or out of a bay, causing a significant change in current speeds when the wind stress relaxes, depending on the phase of the tide and the direction of the wind. Extreme storm surges have a similar effect, and these can be further modified by low atmospheric pressures at the storm's center, which raises water levels. Under exceptional conditions, which are strongly site-specific, these factors can modify local sea levels and influence peak current speeds, as can extended periods of heavy rain and heavy spring melt-water runoff. Although not considered in Phase 1, site-specific analysis of such extreme events must be included in the detailed structural and foundation design of Phase 2.

1.4. Overview of Tidal Stream Energy Conversion Methodology

The instantaneous power density of a flowing fluid incident on a tidal current turbine is given by the following equation:

$$\left(\frac{P}{A}\right)_{Water} = \frac{1}{2}\rho U^3 \qquad \text{(watts per square meter)}$$

where A is the cross-sectional area of flow intercepted by the device, i.e. the area swept by the turbine rotor (in square meters), ρ is water density (in kilograms per cubic meter; 1,000 kg/m^3 for freshwater and 1,025 kg/m^3 for seawater) and U is current speed (meters per second). For tidal currents, U varies with time in a predictable manner as described above, and also depends on depth beneath the water surface and position in the channel, as will be described later.

Because power density varies with the cube of current velocity, it increases quite rapidly with current speed as shown in Figures 1-7 and 1-8.

ρ (kg/m^3)	V (knots)	V (m/s)	P/A$_o$ (W/m^2)
1,025	0.5	0.26	9
1,025	1.0	0.51	70
1,025	1.5	0.77	235
1,025	2.0	1.03	558
1,025	2.5	1.29	1,090
1,025	3.0	1.54	1,884
1,025	3.5	1.80	2,992
1,025	4.0	2.06	4,466
1,025	5.0	2.57	8,722
1,025	6.0	3.09	15,071
1,025	7.0	3.60	23,933
1,025	8.0	4.12	35,725

Figure 1-7 Table of Incident Power Density at Different Current Speeds

As shown in the above table, tidal currents achieve power densities of 500 to 1,000 W/m^2 at flow speeds of 1 to 1.3 m/s (2 to 2.5 knots). Because of the much lower density of air (1.225 kg/m^3 at sea level) relative to water, wind speeds of 9.3 to 11.8 m/s (18 to 23 knots) are required to achieve the same power densities for wind turbines. Appendix A provides a more detailed comparison between tidal stream energy and wind energy.

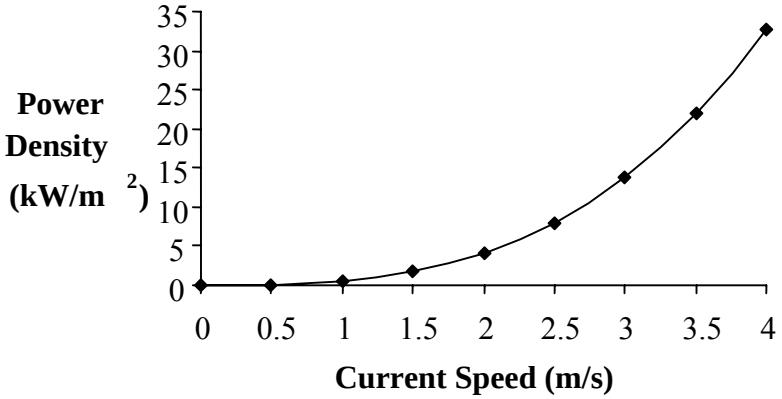

Figure 1-8 Incident Power Density as a Function of Current Speed

Tidal currents vary with time, so currents at a particular site are characterized by a distribution of velocities as shown in Figure 1-9. Since power density varies with the cube of velocity, the mean annual power density cannot be obtained by substituting the mean current speed into the above power density equation.

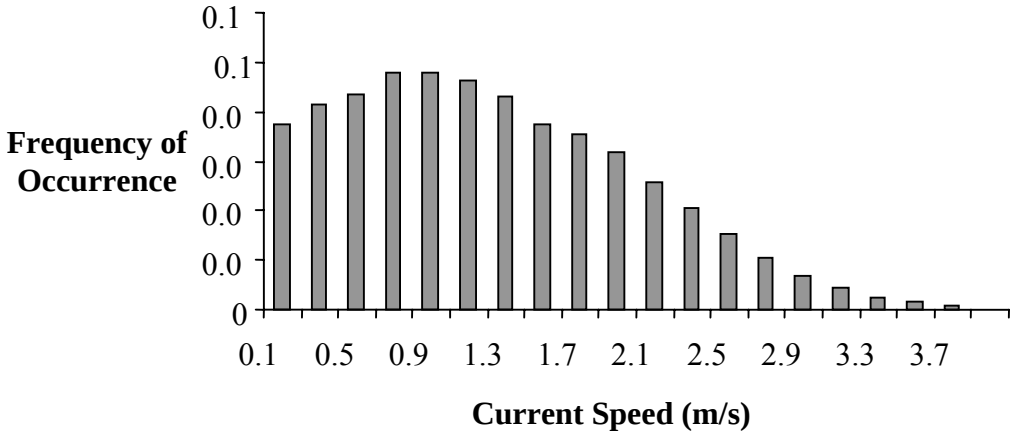

Figure 1-9 Representative Tidal Current Speed Distribution

Once the distribution of velocities is known for a particular site, the distribution of power densities can be readily calculated and averaged to find the average power density for that site. For the example in the above figure, the mean annual power density is 2.2 kW/m^2. Note that the mean annual current speed at this site is 1.2 m/s, which, if simply substituted directly into the power density equation would yield 0.9 kW/m^2, greatly underestimating the resource.

The total power in the flow at a site cannot be extracted for energy production. For water flowing through an unshrouded turbine, maximum extraction efficiency occurs when the flow speed at the rotor face is reduced by 1/3 relative to the free-stream velocity, which yields an optimal extraction efficiency of 16/27 (=59%), which is the so-called "Lanchester-Betz limit." . The extractable energy is further limited by channel geometry and environmental considerations, since the channel cross-section cannot be completely filled with turbine rotors.

- The useable cross-sectional area of a channel is reduced at the top and the bottom of the channel. At the top, navigation clearance requirements will eliminate the upper 15-20 m of water in channels maintained for oceangoing vessels. Elsewhere a 5-m clearance will be required to enable shallow-draft vessels such as commercial fishing boats and deep-keel sailboats to safely travel over the device. At the bottom, the turbine must be above the low-speed benthic boundary layer, which is described later in this section and is typically 1/10 of the mean lower low water (MLLW) depth. The maximum energy that can be extracted is calculated as the mean annual power density multiplied by the useable cross-sectional area between the top and bottom limits described above.
- UK researchers have variously estimated that to minimize the turbine's effect on downstream and upstream environments, the mean annual power extracted should be no more than 10% to 20% of the naturally available physical energy flux (see Section 4.5.2 for documentation). For purposes of this study, EPRI has selected the mid-point between these two estimates, 15%, as the maximum amount of energy that can be extracted from a tidal stream.

Whichever of the above two factors is smaller determines the maximum extractable tidal stream energy resource at a given location. For typical commercial-scale tidal projects at most sites, the 15% environmental extraction constraint will be the limiting factor. This remains to be verified by numerical modeling to simulate energy withdrawal by multiple turbines using computational fluid dynamics and site-specific finite element modeling of channel geometry and bathymetry.

The power recovery efficiency and turbine performance can be estimated using the simplified model of a generic tidal current device described below. The calculation addresses the power conversion efficiency of each step in the process, beginning with the power of the flowing water stream and proceeding through the turbine, drive train, generator and power conditioning steps.

As in the case of wind turbines, turbine efficiency varies with the velocity of water flow. A plot of turbine output as a function of flow speed typically consists of three regions (Figure 1-10).

I. Zero to cut-in speed

II. Cut-in speed to rated speed

III. Greater than rated speed

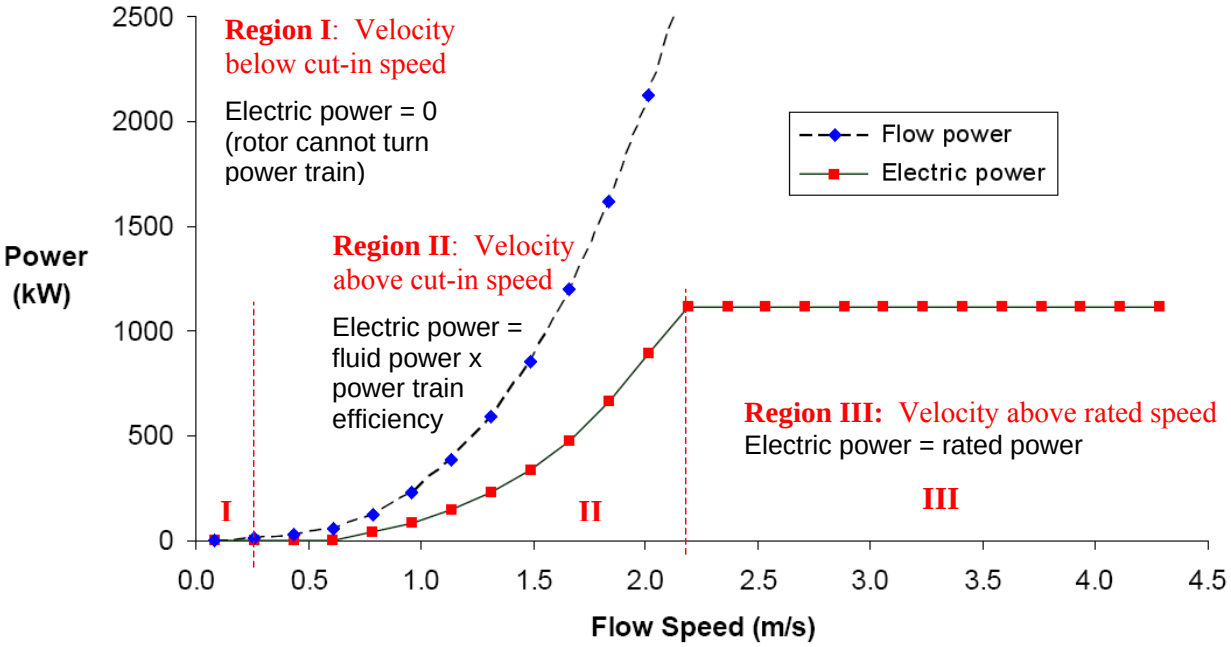

Figure 1-10 Typical Plot of Turbine Output Power vs. Flow Speed

In Region I, at velocities below the cut-in speed, the turbine will not rotate and so generates no power. In Region III, when current velocity exceeds the rated speed of the turbine, power output will be constant, typically at the turbine's rated power, regardless of velocity. Between the cut-in speed and rated speed, in Region II, the turbine's output depends on a chain of "water to wire" conversion efficiencies, as shown in Figure 1-11.

There is no cut-out speed for tidal stream turbines, since even the most extreme currents produced by storm surges superimposed on the highest spring tides are not that much greater than monthly maximum spring tidal currents. This is in contrast to wind turbines, which must be designed to handle the 100-year peak wind speed, which is several times greater than typical monthly maximum wind speeds.

Multiplying the individual efficiencies of the "water to wire" power chain components determines the electric power delivered to the grid, according to the following equation:

$$P_{\text{Delivered Electric}} = A_{\text{Turbine}} \times \left(\frac{P}{A}\right)_{\text{Water}} \times \eta_{\text{TFC}}$$

where

$$\eta_{\text{TFC}} = \eta_{\text{Turbine}} \times \eta_{\text{Drive Train}} \times \eta_{\text{Generator}} \times \eta_{\text{Power Conditioning}}$$

Typical values for component efficiencies when the turbine is operating at its full rating are:

- $\eta_{Turbine} = 45\%$ (maximum theoretically possible is 59%)
- $\eta_{DriveTrain} = 96\%$
- $\eta_{Generator} = 95\%$
- $\eta_{Power\ Conditioning} = 98\%$.

This would result in an overall efficiency of 40%, which is the proportion of incident flow power that would be converted into properly conditioned electric power output.

Finally, it should be noted that the efficiency of different power chain components varies according to the incident flow power, as shown below in Figure 1-11.

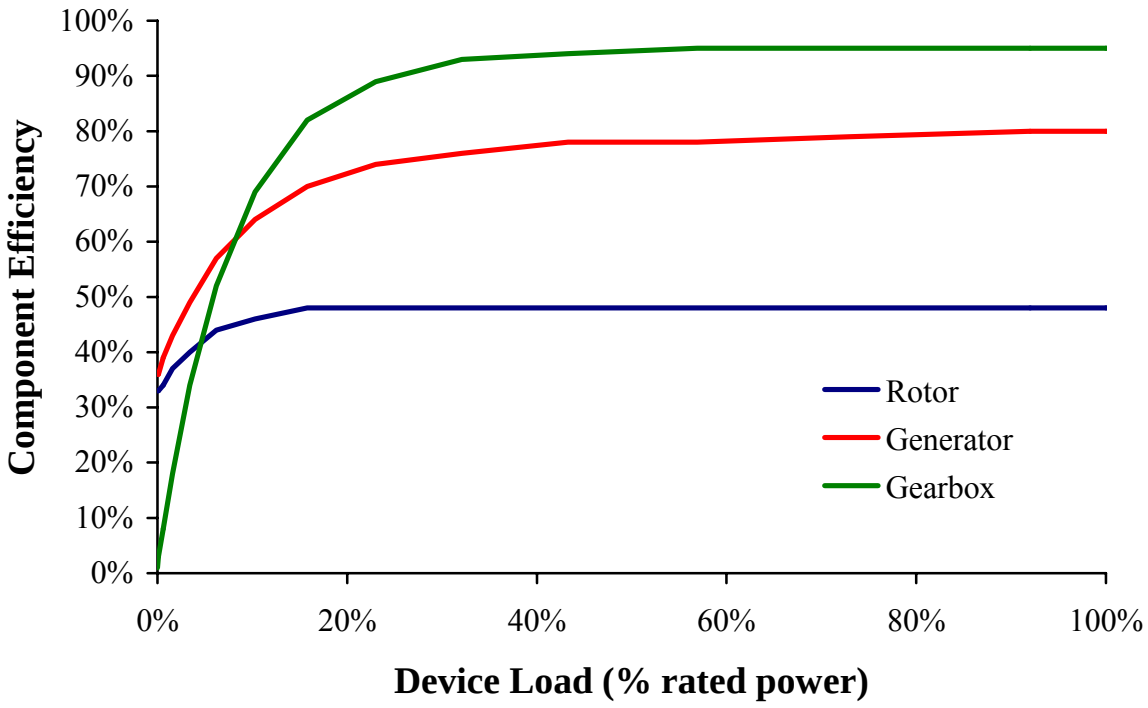

Figure 1-11 Component Efficiency Curves

A tidal current energy conversion device must harness water flow that reverses direction at least once per day and, more commonly, twice per day. Depending on how this is achieved, the above set of curves may differ between flood and ebb current directions. For example, if a tidal stream turbine has a fixed nacelle and reverses the pitch of its blades to handle the reversing flow direction, then the rotor efficiency could change due to the presence or absence of the turbine nacelle in the flow upstream of the rotor.

2. Tidal Current Data Sources

2.1. United States

The National Ocean Service (NOS) Center for Operational Oceanographic Products and Services (CO-OPS) collects and distributes observations and predictions of water levels and currents to ensure safe, efficient and environmentally sound maritime commerce. The center manages the National Water Level Observation Network (NWLON) and a national network of Physical Oceanographic Real-Time Systems (PORTS) in major U.S. harbors. The NOS Tidal Current program is described in Reference 2.

2.1.1. Tidal Current Predictions by the National Ocean Survey (NOS)

Professional mariners and ship operators of all propelled vessels of 1600 gross tons or more are required by the Code of Federal Regulation (33 CFR Chapter I, 7/1/91 Edition, U.S. Coast Guard, DOT '164.01 and '164.33) to carry the current edition of the Tide Tables and the Tidal Current Tables published by the National Ocean Survey (NOS) when operating their vessel in navigable waters of the United States, except in the St. Lawrence Seaway. The tables predict the daily magnitude and timing of high and low water, maximum flood, maximum ebb, and slack for a limited number of representative stations known as reference stations. Predictions at these locations are the basis for predictions at thousands of subordinate, secondary stations through the use of scaling factors and time differences.

NOS tidal predictions page are divided into two sections. The first, Tide Predictions, is posted at http://tidesandcurrents.noaa.gov/tide_pred.html and provides local water level predictions at a few thousand stations around the U.S., Caribbean, and Pacific Islands. The second, Tidal Current Predictions, is posted at http://tidesandcurrents.noaa.gov/currents06/ and provides tidal current prediction for a few hundred U.S. and Canadian tidal current reference stations; as well as time and speed adjustment to allow the calculations to predict tidal currents at a few thousand secondary stations. Both tide and tidal current predictions are provided for the three most recent calendar years. Tide and Tidal Current Predictions are updated in late October or early November to include the next calendar year.

Both tide and tidal current predictions are based upon harmonic analyses of measurements at reference stations. Since extreme weather conditions have been excluded from the analyses and predictions, the predicted values should be considered as those expected under average weather conditions. Tidal water levels are given in feet above Mean Low Water, which is the nautical chart datum of soundings for the U.S., and tidal current speeds are provided in knots.

Unlike tide stations, which are normally located along the shoreline, most tidal current stations are located offshore in the channels, rivers, and bays. Tidal current stations are often named for the channel, river, or bay in which they are located or for a nearby navigational reference point.

2.1.2. Tidal Current Table Formats

The published NOS Tidal Current Tables are presented in the same format as the NOS Tide Tables. A limited number of stations known as reference stations have daily predicted times of floods, ebbs, and slacks and maximum current at floods and ebbs printed in a section known as "*Table 1*". Most tidal current predictions are based on data sets that would be considered inadequate for making tidal water level predictions. Historically, due to technological, logistical, and resource limitations, current measurements are of a shorter duration than water level measurements. The long term continuous operation of the National Water Level Observation Network (NWLON) stations, results in tidal water level constituents that are better resolved and more up to date than the tidal current constituents.

For a larger group of tidal current stations called subordinate stations, predicted floods, ebbs, and slacks are calculated by the user from the "*Table 1*" predictions with time differences and speed ratios. These constants are listed in a section of the Tidal Current Tables known as "*Table 2*". "*Table 2*" also indicates to which tidal current reference station to apply these constants. The constants are obtained by a non harmonic analysis which compares a short period of data at the subordinate station with observations or predictions for the same period at the reference station. The amount of subordinate station data used is usually less than 15 days and in some cases as little as 1 day. Deciding which reference station to use for a subordinate station is a subjective decision usually based on proximity and similarity in the shapes of the tidal current curves.

Data from primary tidal current reference stations are the source for computing accepted values of harmonic constituents and non-harmonic constants essential to daily tidal current predictions. Existing tidal current predictions are presently based on limited data sets from reference stations that date as early as 1901. The data from these stations serve as the control for the reduction of short time series from subordinate current stations through comparison of simultaneous observations. Historically, reference stations require a minimum of 15 days of continuous velocity measurements for harmonic analysis from which subordinate stations predictions can be computed with time differences and speed ratios. Longer time series improve predictions at reference stations by enabling resolution of similar harmonic constituent frequencies.

2.1.3. U.S. Geographical Coverage

NOS reference stations for tidal current prediction in the five U.S. regions of interest, that is, Cook Inlet Alaska, Puget Sound Washington, San Francisco Bay California, Bay of Fundy Maine, and Massachusetts, are shown in Figure 2-1.

2.1.4. Characteristics of Primary Tidal Current Reference Stations

Table 2-1 provides a list of characteristics for primary tidal current reference stations in the five U.S. states covered by this study. The number of harmonic constituents used to make tidal current predictions varies between eight at the Bay of Fundy Entrance, and twenty-nine at Carquinez Staits in the San Francisco Bay area, California. Predictions for the Bay of Fundy Entrance are provided by the Canadian Hydrographic Service and are included in this study because 135 U.S. subordinate (secondary) prediction stations are referenced to it.

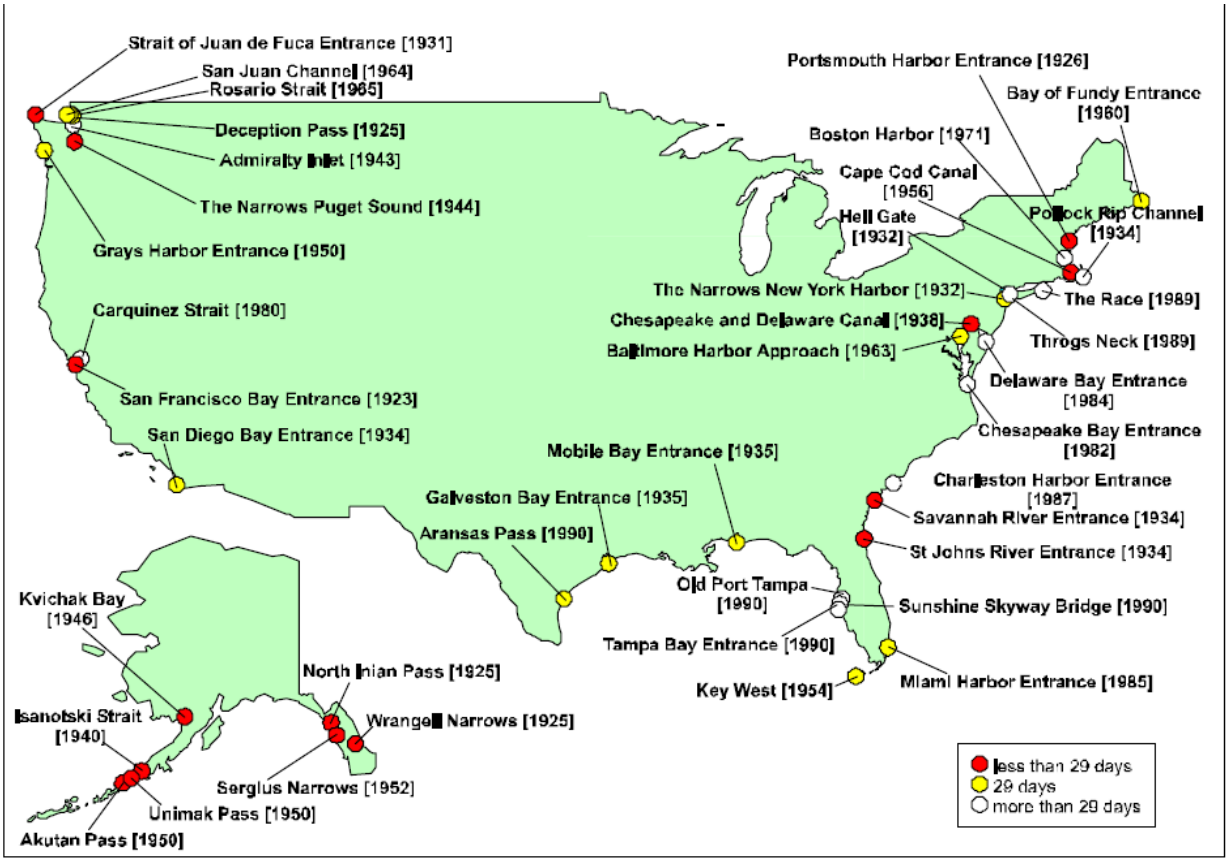

Tidal current reference stations of the United States categorized by duration of observations with the year of data acquisition in brackets.

Figure 2-1. Map of Primary U.S. Tidal Current Reference Stations

The maximum flood currents (MFC) and maximum ebb currents (MEC) shown in Table 2-1 are the average of the greatest speeds during a flood or an ebb period. They provide an estimate of the strength of current at the reference stations which were usually chosen to be located where the strongest currents in a bay or estuary could be measured. The volume of water that must pass a given point in a bay or estuary is equal to the tidal prism above that location. The tidal prism is approximately the surface area of the bay multiplied by the mean tidal range of the bay. Tidal currents will be proportional to the tidal prism and inversely proportional to the cross sectional area through which the volume of water must pass. The strongest currents (> 5 knots) occur in narrow channels or channels through which large volumes of water must pass (Deception Pass, Sergius Narrows, and Akutan Pass). The weakest currents (< 1 knot) occur in wide or deep channels (main basin of Puget Sound) or at some distance from the ocean.

Table 2-1

U.S. Tidal Current Reference Stations in AK, WA, SF, MA, and ME

Reference Station Name	Number of Subordinate Stations	Number of Constituents	MFC Speed (knots)	MEC Speed (knots)	Permanent Current (knots)	Tidal Ratio	Tidal Class-ification
Bay of Fundy Entrance (Canada)	135	8	2.3	2.4	-0.041	0.09	S
Boston Harbor, MA	153	13	1.1	1.2	-0.280	0.15	S
Cape Cod Canal, MA	16	17	4.0	4.5	0.000	0.10	S
Pollock Rip Channel, MA	115	16	2.0	1.8	0.150	0.08	S
San Diego Bay Entrance, CA	27	16	1.2	1.5	-0.090	0.36	M M S
San Francisco Bay Entrance, CA	136	20	2.9	3.4	-0.200	0.38	M M S
Carquinez Strait, CA	57	29	2.1	2.2	-0.138	0.51	M M S
Grays Harbor Entrance, WA	44	20	1.9	2.8	-0.300	0.30	M M S
Strait of Juan de Fuca Entrance, WA	1	14	0.6	1.5	-0.500	0.53	M M S
Admiralty Inlet, WA	75	17	1.6	2.6	-0.500	0.53	M M S
The Narrows Puget Sound, WA	31	20	3.2	2.8	0.000	0.44	M M S
Deception Pass, WA	4	17	5.2	6.6	-0.650	0.29	M M S
Rosario Strait, WA	46	20	1.1	1.9	-0.400	0.70	M M S
San Juan Channel, WA	13	21	2.6	2.6	-0.050	0.50	M M S
Wrangell Narrows, AK	345	21	3.7	3.4	0.000	0.16	S
Sergius Narrows, AK	62	18	5.9	5.5	0.200	0.06	S
North Inian Pass, AK	28	21	2.9	5.1	-1.400	0.17	S
Isanotski Strait, AK	11	18	3.6	2.8	0.400	0.36	M M S
Unimak Pass, AK	35	20	3.4	3.0	0.500	0.72	M M S
Akutan Pass, AK	7	21	5.8	5.3	0.200	0.56	M M S
Kvichak Bay, AK	39	17	2.5	2.5	-0.300	0.29	M M S

S = Semidiurnal, M M S = Mixed Mainly Semidiurnal, M M D = Mixed Mainly Diurnal, D = Diurnal

The Tidal Ratio in the next-to-last column of Table 1-2 is the ratio of the amplitudes of the largest diurnal constituents to the largest semidiurnal constituents, classifying the tides as semidiurnal (S; ratio < 0.25), mixed mainly semidiurnal (MMS; 0.25 < ratio < 1.5), mixed mainly diurnal (MMD; 1.5 < ratio < 3.0), or diurnal (D; ratio > 3.0). A subordinate station should be associated with a reference station that has a similar tidal ratio. Table 1 identifies each of the reference station's tidal characteristics based on the tidal ratio. All of the east coast of the U.S. is semidiurnal with the exception of Baltimore Harbor Approach and Chesapeake & Delaware Canal, which are mixed mainly semidiurnal. All of the reference stations in California and Washington are mixed mainly semidiurnal. In Alaska, the southeastern stations are semidiurnal while the southwestern stations are mixed mainly semidiurnal.

2.1.5. Example Tidal Current Table Data

The availability of tidal current predictions and observed current data is limited compared to the availability of tide level data. Continuous measurements of currents were not possible until recently. Archived data sets are available but data quality can vary considerably based on the age of the data and location of the measurements. Data from the last 30 years is in digital form; older data exists as paper transcripts. Inquiries about specific locations to ascertain if data exists, its quality and availability will be answered by the NOS office at (301) 713-2815 between 7AM-3PM Eastern Time or via e-mail at: Tide.Predictions@noaa.gov

Short-term tidal current predictions for a single calendar month at any of the primary or secondary stations listed in the Tidal Current Predictions section of the NOS web site can be obtained via e-mail request to: Tide.Predictions@noaa.gov. Subsequent requests for additional months will be subject to the fee for custom predictions described below.

Long-term tidal current predictions (more than 1 month) can be obtained on a calendar year basis by calling the NOS office at (301) 713-2815 between 7AM-3PM Eastern Time or via e-mail request to: Tide.Predictions@noaa.gov.

Tidal current predictions are available in several different formats.

- *International Format* - This format is an electronic ASCII file which provides time and speed of current for a single location in a column delimited format. This format is most suitable for importing into a database, plotting, or other computer program.
- *Standard Format* - This format is available in hardcopy and as an electronic ASCII file which provides time and speed of current for a single location in a page readable format. The following example for San Francisco, CA, February, 2004 (shown in Table 2-2), gives the predictions in Pacific Standard Time using 24-hour notation.
- *Manuscript Format* - This format is available in hardcopy and as an electronic PostScript file, which provides time and speed of current for a single location in a 3-month per page format. This format includes additional information such as the day of week and phases of the moon.

Table 2-2

Example Tidal Flow Prediction Data for San Francisco February 2004

San Francisco Bay Entrance (Outside), California

Predicted Tidal Current February, 2004

Flood Direction, 65 True. Ebb (-)Direction, 245 True. NOAA, National Ocean Service

	Slack Water	Maximum Current		Slack Water	Maximum Current		Slack Water	Maximum Current		Slack Water	Maximum Current	
Day	Time	Time	Vel	Time	Time	Veloc	Time	Time	Veloc	Time	Time	Veloc
	h.m.	h.m.	knots	h.m.	h.m.	knots	h.m.	h.m.	knots	h.m.	h.m.	knots
1		44	-1.2	352	641	1.8	922	1247	-3.8	1700	2015	2.9
2		137	-1.3	439	727	2.0	1009	1334	-4.1	1744	2056	3.2
3	6	217	-1.5	521	810	2.2	1053	1417	-4.4	1824	2133	3.4
4	45	253	-1.7	559	849	2.4	1135	1457	-4.6	1901	2205	3.5
5	122	330	-2.0	636	928	2.6	1215	1536	-4.8	1936	2236	3.6
6	156	407	-2.2	714	1007	2.7	1254	1615	-4.8	2009	2307	3.6
7	229	446	-2.5	753	1048	2.7	1335	1655	-4.7	2041	2340	3.6
8	302	526	-2.8	837	1131	2.7	1419	1736	-4.4	2114		
9		14	3.5	334	609	-3.1	925	1219	2.7	1510	1821	-4.0
10		52	3.3	406	654	-3.4	1019	1312	2.6	1609	1909	-3.4
11		134	3.0	442	742	-3.6	1121	1412	2.5	1719	2003	-2.7
12		222	2.6	523	836	-3.8	1230	1521	2.5	1840	2103	-2.1
13	5	316	2.3	611	934	-4.0	1342	1638	2.6	2005	2209	-1.7
14	113	419	2.1	709	1037	-4.2	1452	1759	3.0	2122	2321	-1.5
15	229	525	2.1	812	1143	-4.5	1555	1908	3.4	2228		
16		34	-1.6	339	631	2.4	916	1246	-4.9	1653	2006	3.8
17		138	-1.9	439	732	2.7	1017	1344	-5.2	1745	2056	4.1
18	10	231	-2.3	533	826	3.0	1113	1437	-5.4	1833	2140	4.3
19	52	317	-2.6	623	917	3.3	1206	1524	-5.4	1916	2220	4.3
20	131	359	-2.9	711	1004	3.4	1256	1608	-5.1	1957	2258	4.1
21	208	439	-3.2	758	1050	3.4	1346	1650	-4.7	2036	2333	3.8
22	243	518	-3.4	846	1137	3.2	1435	1731	-4.1	2114		
23		9	3.4	317	558	-3.4	935	1224	2.9	1527	1814	-3.4
24		45	2.9	352	640	-3.4	1027	1315	2.6	1622	1858	-2.7
25		124	2.4	427	724	-3.3	1124	1411	2.3	1725	1947	-2.1
26		208	1.9	507	813	-3.1	1227	1519	2.0	1837	2042	-1.5
27	12	301	1.5	553	908	-3.0	1335	1641	2.0	1953	2146	-1.1
28	122	403	1.3	650	1009	-3.0	1441	1759	2.2	2105	2259	-1.0
29	232	511	1.3	752	1114	-3.2	1540	1900	2.5	2205		

All times listed are in Local Time, and all speeds are in knots.

2.1.6. Tidal Current Prediction Software

A variety of tidal prediction programs are available as freeware on the Web or as commercial programs available for purchase. An example freeware program is *WXTide32*, which is available at http://www.wxtide32.com/download.html. An example commercial program is Nobeltec Navigation's *Tides & Currents*, described at http://nobeltec.com/products/prod_tides.asp and available for sale (lists at $129) from suppliers of electronic charting products.

2.2 Canada

2.2.1. Canadian Hydrographic Service (CHS) Publications

The Tides, Currents, and Water Levels Web Site (http://www.waterlevels-niveauxdeau.gc.ca/) provides predicted times and heights of high and low waters, and the hourly water levels for over seven hundred stations in Canada. Presently, there are no current predictions available on the web site. A printed version is published yearly and is available from authorized CHS chart dealers. The printed Canadian Tide and Current Tables come in seven different volumes covering the regions shown in Figure 2-2.

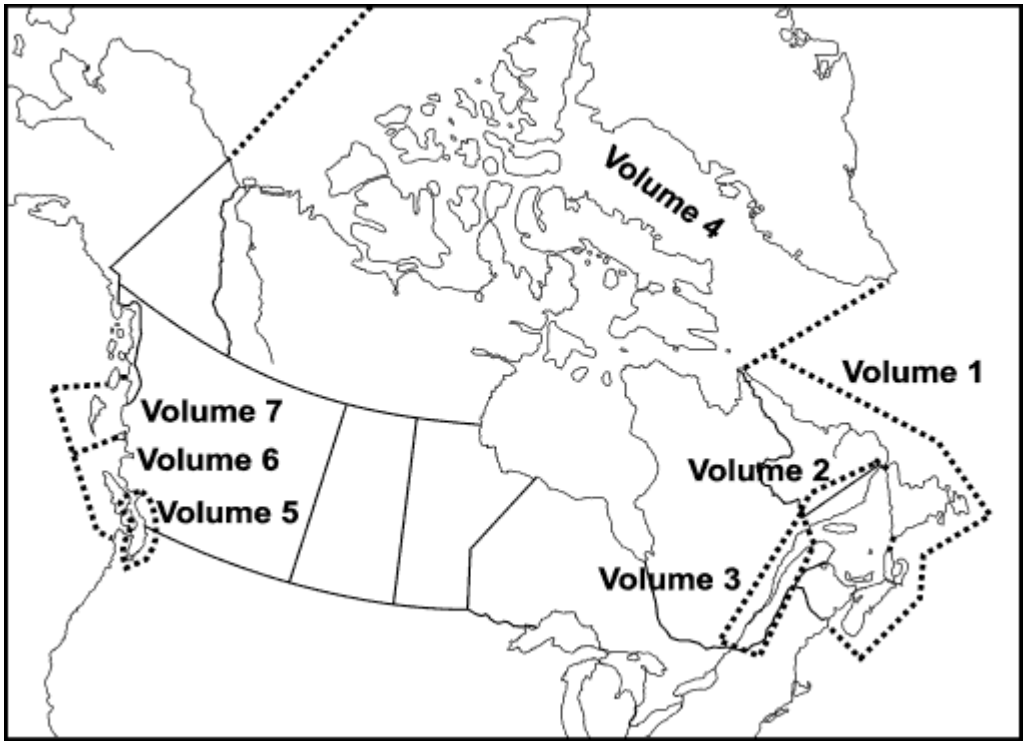

Figure 2-2 Regions covered by the Canadian Tide and Current Tables

It should be noted that Volume 2 of the Tidal Current Tables (Reference 3) covers only three stations in Atlantic Canada: Grand Manan Island (at the entrance to the Bay of Fundy), Abgeweit Passage (between Nova Scotia and Prince Edward Island), and the Great Bras D'Or Channel entrance (on the north coast of Cape Breton Island).

Printed Tidal Current Atlases also are available, which present a comprehensive view of the hourly rate and direction of major tidal currents within specific coastal regions of Canada. These Atlases use arrows to indicate the direction and the velocity of surface currents. They are intended for use in conjunction with the CHS Tide and Current Tables and are available for the Bay of Fundy and Gulf of Maine (Reference 4), St. Lawrence Estuary from Cap de Bon-Désir to Trois-Rivières, and Juan de Fuca Strait to Strait of Georgia on the Pacific Coast.

2.2.2. Department of Fisheries and Oceans (DFO) Software – *WebTide*

Because CHS current tables exist for only three sites in Atlantic Canada, EPRI used the freely available *WebTide* software package to develop tidal current time histories at the sites selected for conceptual design by the NB and NS Advisory Groups. *WebTide* is a graphical user interface to a tidal prediction program covering the ocean regions shown in Figure 2-3, developed by the Bedford Institute of Oceanography and maintained by the Department of Fisheries and Oceans (http://www.mar.dfo-mpo.gc.ca/science/ocean/coastal_hydrodynamics/WebTide/webtide.html). Predictions can be obtained for any geographic coordinates inside a selected model domain and are based upon analyses on the output from a variety of ocean models.

WebTide is based on a relatively coarse numerical grid. Several Canadian experts have told EPRI that *WebTide* was never intended to yield accurate tidal current velocities in nearshore, constricted passages. Even so, it was the only tool available to develop velocity time histories at the selected NB and NS sites. Details of these site-specific calculations and their results are presented in Section 4 of this report

The EPRI approach was to use *WebTide* to "hindcast" tidal current velocities at a location and time period of nearby short-term measurements, and then use those data to develop regression relationships for adjusting *WebTide* velocities at that location, applying those adjustments to a year-long hindcast at the nearby TISEC transect selected by our NB and NS stakeholders.

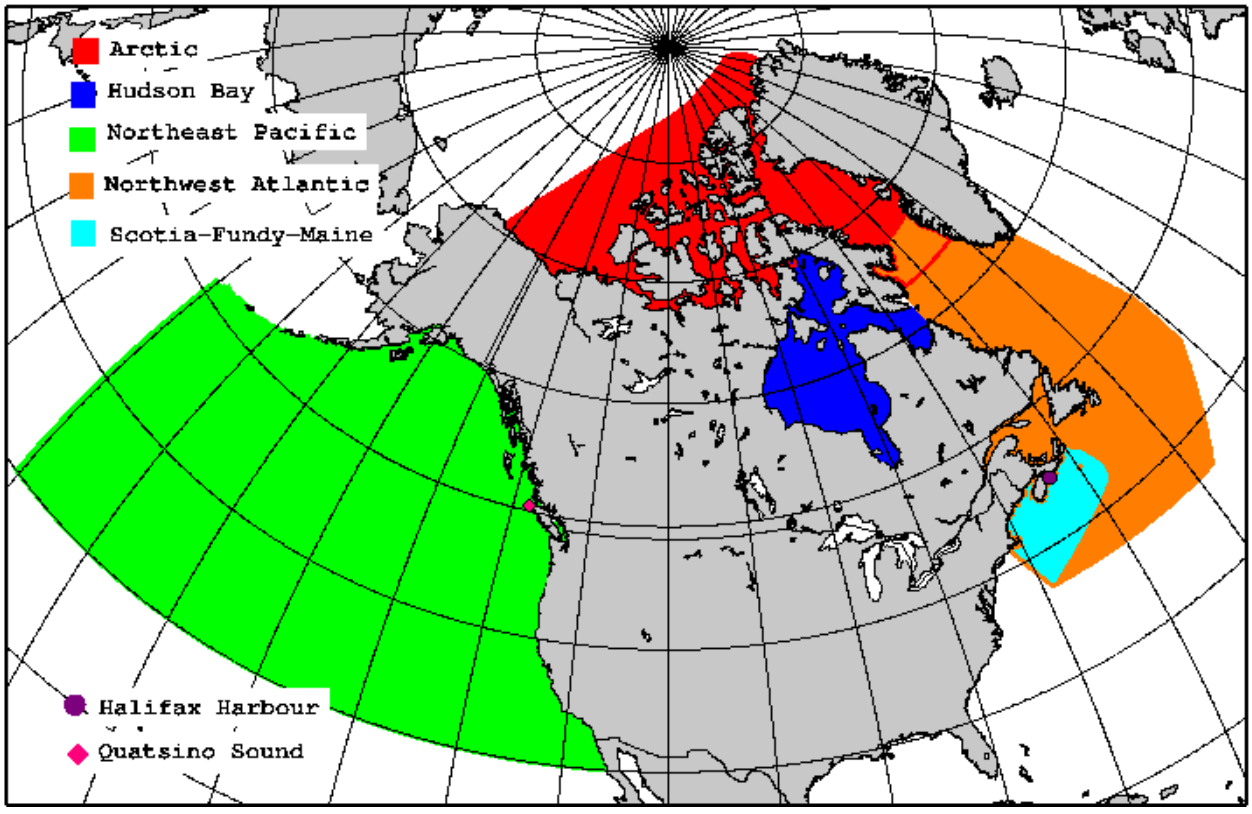

Figure 2-3 *WebTide* Ocean Model Regions

3. Tidal Stream Resource Methodology for Site Survey Reports

This section describes the methodology used by EPRI to calculate the total mean annual tidal stream energy resource available and extractable at the many North American east coast sites in Massachusetts, Maine, New Brunswick and Nova Scotia, as documented in the four Tidal Power (TP-) 003 Site Survey Reports posted at http://www.epri.com/oceanenergy/streamenergy.html. The purpose of these calculations was to enable the Advisory Groups in MA, ME, NB, and NS to objectively compare the tidal stream energy resources among a short list of six to ten sites in each state or province.

Section 4 describes the methodology used to calculate average power output and annual energy production for the TP 006 Design Reports that were produced for seven selected sites in Alaska, Washington State, San Francisco, and the four east coast states and provinces listed above.

3.1. Site Screening

Potential TISEC sites typically are found where there is a narrow channel or passage between two landmasses, or an inlet into a bay, through which substantial volumes of tidal water must flow. Among the many attributes of a potential TISEC project site is the size of the tidal stream resource, which is a function of both the speed of the tidal currents (incident power density) and the channel cross-sectional area (width and depth). As detailed in the Site Survey Reports, the site also should have suitable seabed geology for proper anchoring of the TISEC devices, and it should be situated reasonably close to an existing grid interconnection point and a shoreside support center with a suitable harbor for inspection, maintenance and repair.

Initial screening of sites for inclusion in the Site Survey reports was based on peak ebb and flow velocities reported in tidal current tables or shown as vectors on hydrographic charts. Any site that had either flood or ebb peak currents averaging at least 3 knots (1.5 m/sec) was included in the Survey Report. Sites also were included if there was anecdotal evidence for high tidal flow speeds, even when the 3-knot peak speed criterion was not met. For example, CHS hydrographic charts for Cape Enrage show tidal current vectors of only 2 knots, but multi-beam imagery of the seabed shows several features (sand waves, scour channels) that suggest stronger flows (see NB Site Survey report for details).

3.2. Mean Annual Power Density

To estimate the mean annual power density, it is first necessary to know the speed of the surface currents as a function of time, which is available from a variety of data sources, as previously reviewed in Section 2. The calculation must then account for the vertical variability of current speed with depth, and its horizontal variability across the channel. This yields an estimate for the mean annual, depth-averaged, width-averaged tidal stream power density. Multiplying this estimate by the channel cross-sectional area yields an estimate of the mean annual incident tidal stream power, which is the available physical resource. As previously mentioned, only a fraction of this (15%) can be withdrawn in order to limit environmental effects, and this is the extractable resource. The basis for this 15% limit is documented in Section 4.5.3.

3.2.1 Surface Current Velocities

Surface current velocities for the east coast sites surveyed were obtained from the best available data. For most U.S. locations, these were predictions from the NOS Tidal Current Tables, where they were available. NOS predictions were available for all six sites surveyed in Massachusetts, but only for five out of the ten sites surveyed in Maine.

For the eleven U.S. sites where NOS predictions were available, the commercial software program, *Tides & Currents* (see Section 2.1.6, above) was used to predict the surface velocity time history for the entire calendar year of 2005, at 30-minute intervals. A probability distribution analysis was then performed on this time history to create a histogram showing how frequently particular speed categories occurred throughout that year.

Among the five remaining Maine sites, there were no surface current data available for three of them, there was a year of measured data available from a moored buoy in Outer Cobscook Bay (see ME Site Survey Report for details), and there were some instantaneous numerical modeling snapshots (from References 5 and 6) for Lubec Narrows, which were consistent with anecdotal reports in the U.S. *Coast Pilot* (Reference 7).

For the year of data available from the GoMOOS buoy in Outer Cobscook Bay, a probability distribution analysis was performed to create a histogram showing how frequently particular speed categories occurred throughout that year. A detailed description of this analysis is given in Section 3.3.1 of the ME Site Survey Report.

For most Canadian locations, the primary surface current data were the peak velocity vectors indicated on CHS hydrographic charts (see Site Survey Reports for details). This was not true of Head Harbour Passage and Letete Passage in New Brunswick, where only anecdotal references to peak currents were available, from the CHS *Sailing Directions*. (Reference 8), but these appeared to be consistent with the numerical model of Passamaquoddy and Cobscook Bays by Brooks (References 5 and 6). This also was not true for the St. John River below Reversing Falls in New Brunswick, where no data were available. Two Maine sites – Western Passage and Lubec Narrows – are shared with New Brunswick, and the surface current estimates from the ME Site Survey Report were used for the NB report as well.

For Lubec Narrows (in ME and NB) and for all the Canadian sites (except St. John River, for which no data were available), only the surface current peak velocities were available, which were used to calculate the peak power density, using the equation given in Section 1.4, above.

It was assumed that these represented average conditions (midway between spring and neap tides), and the year-long time history of surface current velocity could be approximated by a sine wave having an amplitude equal to this average peak. For such a sine wave, the time-averaged value of the absolute speed over one year would be 63.7% of the peak speed. Moreover, the mean value of the speed-cubed would be 42.4% of the peak speed-cubed. Therefore, the mean annual tidal current power density at the surface was estimated as 0.424 times the power density estimated for the average peak currents. It is recognized that this is a very coarse approximation, not suited for turbine performance estimates. For site comparison purposes, however, it is considered to provide a reasonable indicator of the relative TISEC resource at each site.

3.2.2 Accounting for Velocity Variability with Depth

The depth-averaged tidal stream power density was estimated from the surface value by annual assuming a 1/10th power law approximates the decrease in current velocity from the sea surface to the bottom of the channel (see Figure 3-1 for comparison with other possibilities).

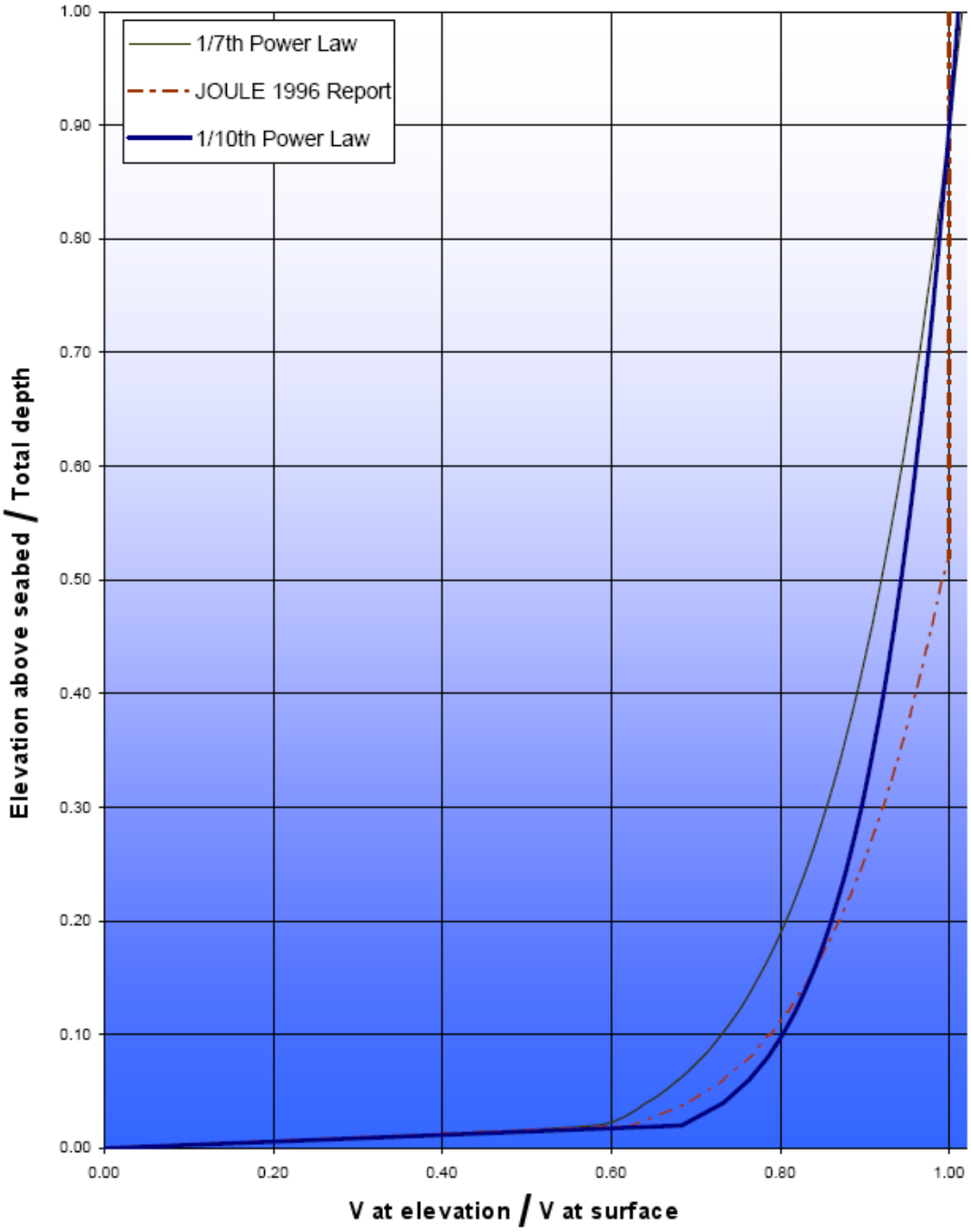

Figure 3-1 Alternative Profile Formulations of Velocity Variability with Depth (1/10th-Power Law used for this study)

The general power law relationship for vertical profiles of horizontal fluid flow velocity near a solid boundary (the seabed, for example) is as follows:

$$u(z) = u_o\left(\frac{z}{z_o}\right)^{1/10}$$

where *u(z)* is the horizontal velocity at some depth *z*, and u_o is the reference velocity at a reference depth (z_o). Depths are measured relative to the bottom, such that the seabed is at *z*=0. Based on the 1/10-power law velocity profile, the depth-averaged value of velocity is 90.9% of its surface value - the derivation of which is given below.

For any reference velocity and depth, the depth-averaged velocity is given by

$$\bar{u} = \frac{\int_{h_1}^{h_2} u\,dz}{\int_{h_1}^{h_2} dz} = \frac{\int_{h_1}^{h_2} u_o\left(\frac{z}{z_o}\right)^{1/10} dz}{\int_{h_1}^{h_2} dz} = \frac{u_o\left(\frac{1}{z_o}\right)^{1/10}}{h_2 - h_1}\left(\frac{10}{11}\right)\left(h_2^{11/10} - h_1^{11/10}\right)$$

When the reference velocity is the surface velocity, then:

h_2 = channel depth (D),

h_1 = 0,

z_o = reference elevation = h_2 at the surface, and

the depth averaged velocity is:

$$\bar{u} = \frac{u_o\left(\frac{1}{D}\right)^{1/10}}{D}\left(\frac{10}{11}\right)\left(D^{11/10} - 0^{11/10}\right) = u_o\left(\frac{10}{11}\right) = 0.909u_o$$

Since flow power density is proportional to the cube of flow velocity, then an expression for the depth-averaged power density can be derived in a similar fashion:

$$\overline{u^3} = \frac{\int_{h_1}^{h_2} u^3\,dz}{\int_{h_1}^{h_2} dz} = \frac{\int_{h_1}^{h_2} u_o^3\left(\frac{z}{z_o}\right)^{3/10} dz}{\int_{h_1}^{h_2} dz} = \frac{u_o^3\left(\frac{1}{z_o}\right)^{3/10}}{h_2 - h_1}\left(\frac{10}{13}\right)\left(h_2^{13/10} - h_1^{13/10}\right) = u_o^3\left(\frac{10}{13}\right) = 0.769u_o^3$$

Therefore, the depth-averaged tidal current power density at each site surveyed was estimated as 76.9% of the mean annual surface power density, which as noted previously was estimated as 42.4% of the power density estimated for the average peak surface currents.

3.2.2 Accounting for Velocity Variability Across Channel

It was assumed that velocity is constant across the width of the channel. This overestimates the available resource, since currents close to shore will be slower than in mid-channel. This was a necessary approximation in the absence of other data, however, and should not affect the relative resource ranking of sites surveyed.

3.3 Channel Cross-Sectional Area

To estimate the channel cross-sectional area, a transect was drawn across the channel on a bathymetric chart or hydrographic chart of soundings. This transect was divided into sections, where the section width was chosen to capture the complexity of cross-channel bathymetry: many narrow sections to capture rapidly changing bathymetry, but only a few wide sections to capture flat or gradually changing bathymetry (see Figure 3-2). For each section, the area of the trapezoid between section boundaries is calculated, and the results summed for all sections.

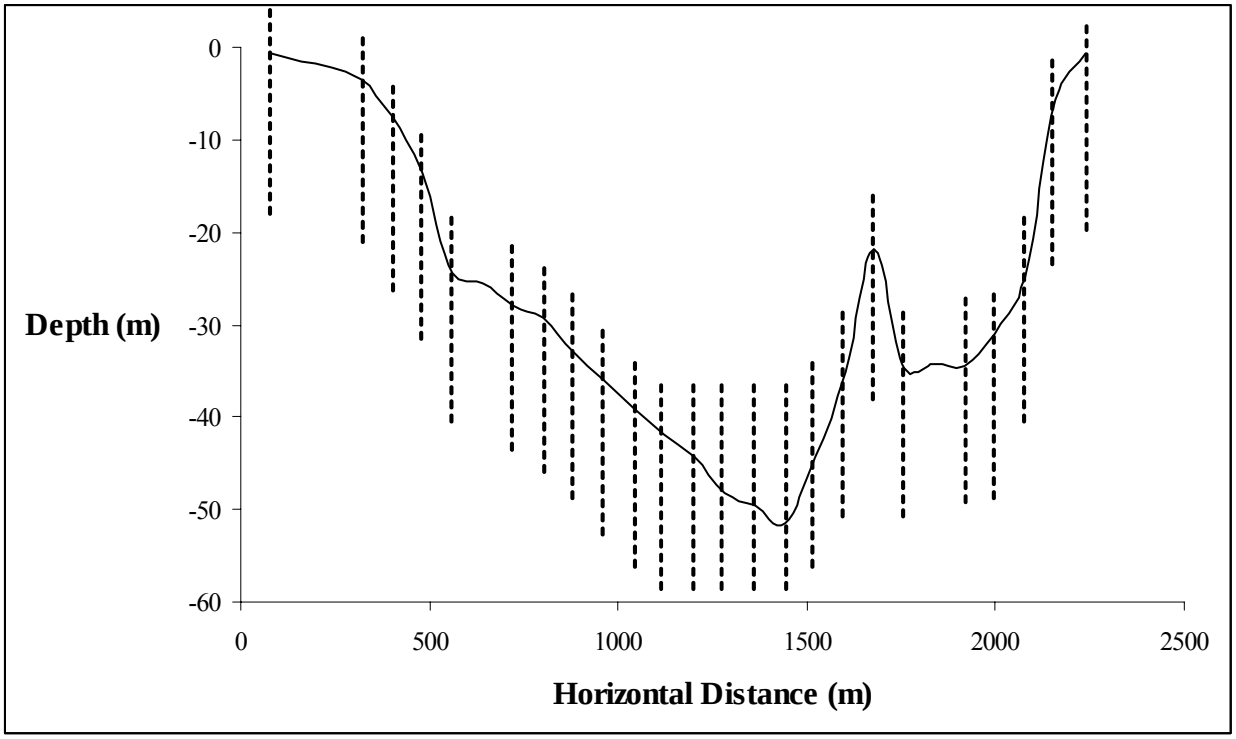

Figure 3-2 Cross-Section of Tidal Channel (dotted lines show section boundaries)

The chart datum (shoreline elevation) for depth contours or soundings as reported from NOAA or USGS is typically Mean Lower Low Water (MLLW). MLLW is defined as the annual average of the daily lower low tides. To this subtidal channel area was added a rectangular area, whose width was the channel width (shoreline to shoreline) at MLLW, and whose height was half of the mean tidal range (Figure 3-3). This combination approximates the average cross-sectional flow area and also the flow area at mid-tide, when current speeds usually are greatest.

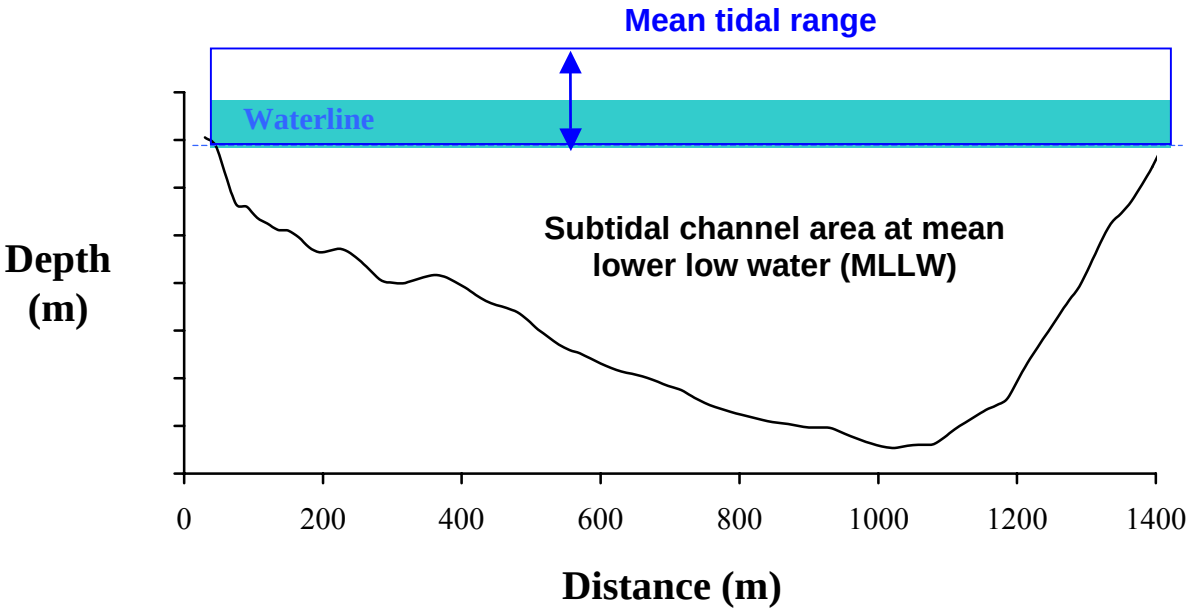

Figure 3-3 Accounting for Tidal Range in Cross-Sectional Area Calculation

3.4 Total Available Resource

The total available tidal stream resource is the product of the mean annual, depth-averaged power density (as calculated per Section 3.2) times the mean channel cross-sectional area (as calculated per Section 3.3). This yields the mean annual kinetic tidal power.

3.5 Extractable Resource

As mentioned earlier, environmental concerns were assumed to limit the mean annual extractable power to 15% of the mean annual kinetic power. The basis for this assumption is documented in Section 4.5.2, at the end of this report.

4. Tidal Stream Power Production Methodology for Design Reports

Although approximate tidal stream resource estimates based on peak current speeds were adequate for site comparison in the TP-003 Site Survey Reports, a much more accurate representation of the local flow velocity time history is required for conceptual design. This is needed not only to properly characterize the site-specific energy resource, but also to identify the maximum current speed that structures and foundations must be designed to withstand.

4.1. Surface Current Velocity Distribution

Unlike wind speeds, which are stochastic in nature and can be represented by generalized probability distribution functions such as the Weibull distribution, tidal current speeds are governed by strongly site-specific deterministic harmonic constituent functions, such that a generalized probability distribution function cannot be applied. The only way to generate the required velocity distribution is to generate a site-specific time history of tidal current speeds and run a histogram analysis to determine how the speeds are distributed at that site.

Among the seven different sites for which conceptual TISEC project designs were developed, there were a variety of different approaches to developing the surface current velocity time history. For all sites, tidal current predictions for 2005 were used, and the time histories were of 30-minute average surface velocities. This resulted in 17,520 data points, which were then sorted into speed categories to generate a histogram showing their probability distribution.

For the sites in Alaska (AK) and Washington (WA), the NOS Tidal Current Tables were used to construct a surface velocity time history according to the procedure described in Section 4.1.1.

For the sites in San Francisco (SF), Massachusetts (MA) and Maine (ME), the commercial software package *Tides & Currents* described in Section 2.1.6 was used to generate the surface current velocity time history. In SF and ME, however, the tidal current prediction station was not located at the project site, which is at a location where the channel is narrower and therefore the currents faster. In these two cases, open-channel flow theory was used to derive the velocities based on the ratio of channel cross-sectional areas between the prediction station and the project site, as described in Section 4.1.2.

For the two Canadian sites, the free *WebTide* software package described in Section 2.2.2 was used to generate the surface current velocity time history, after first "calibrating" its output with a nearby short-term measurement site. Because the nature of this calibration was significantly different between the site in New Brunswick and the site in Nova Scotia, the procedures are described separately, in Sections 4.1.3 and 4.1.4.

Figures 4-1 and 4-2 show the probability distribution histograms for tidal current speeds at five of the conceptual design sites: MA, ME, and NS on the east coast, and WA and AK on the west coast. The much larger diurnal inequality on the west coast causes at least two relatively low peaks per day, which broadens the distribution and pulls its modal velocity toward the lower end. Peak velocities are more similar from tide to tide in the semi-diurnal tidal regimes on the east coast, yielding a narrower distribution with the modal velocity shifted towards the upper end.

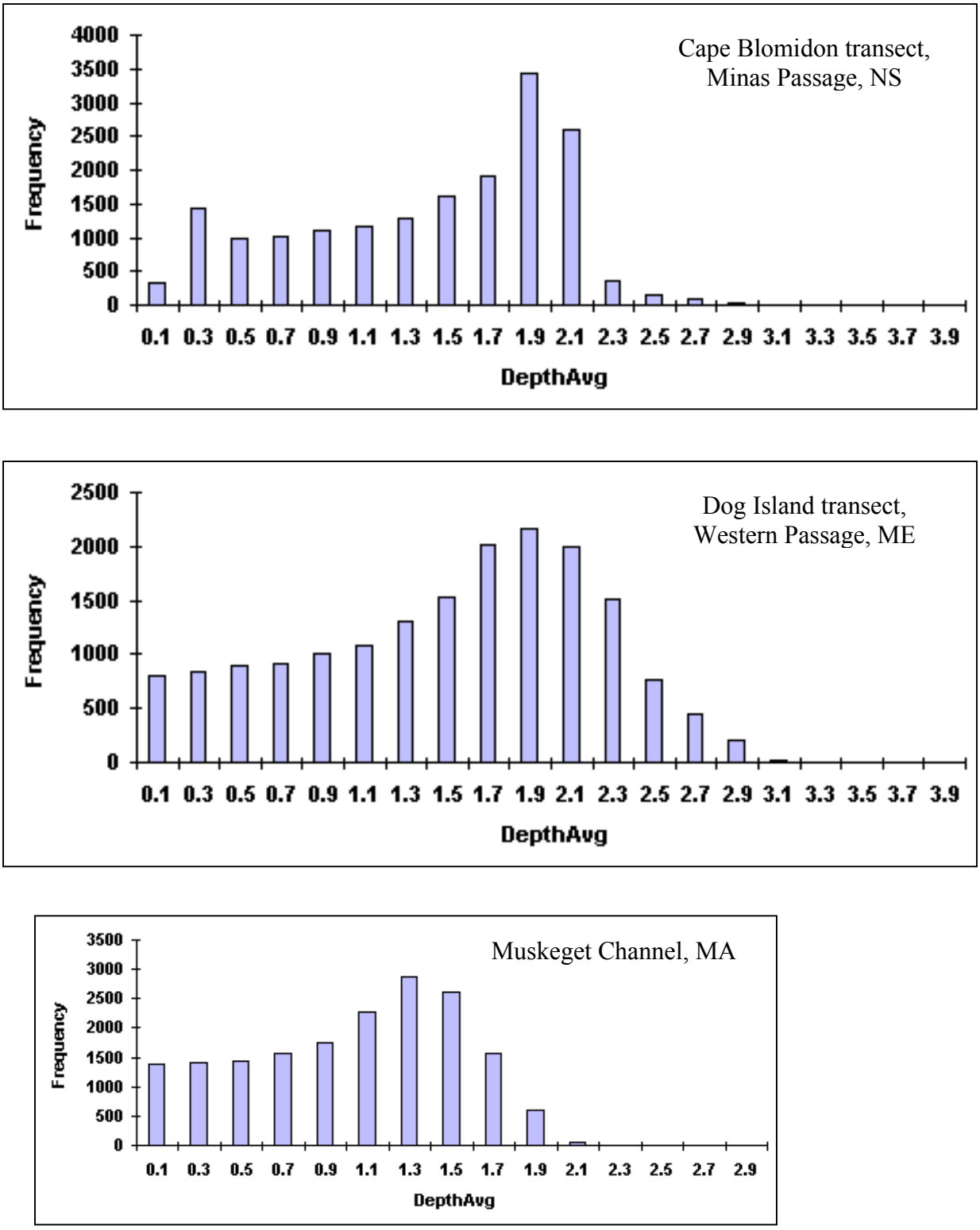

Figure 4-1. Depth-Averaged Tidal Current Speed Probability Distributions for North American East Coast Sites

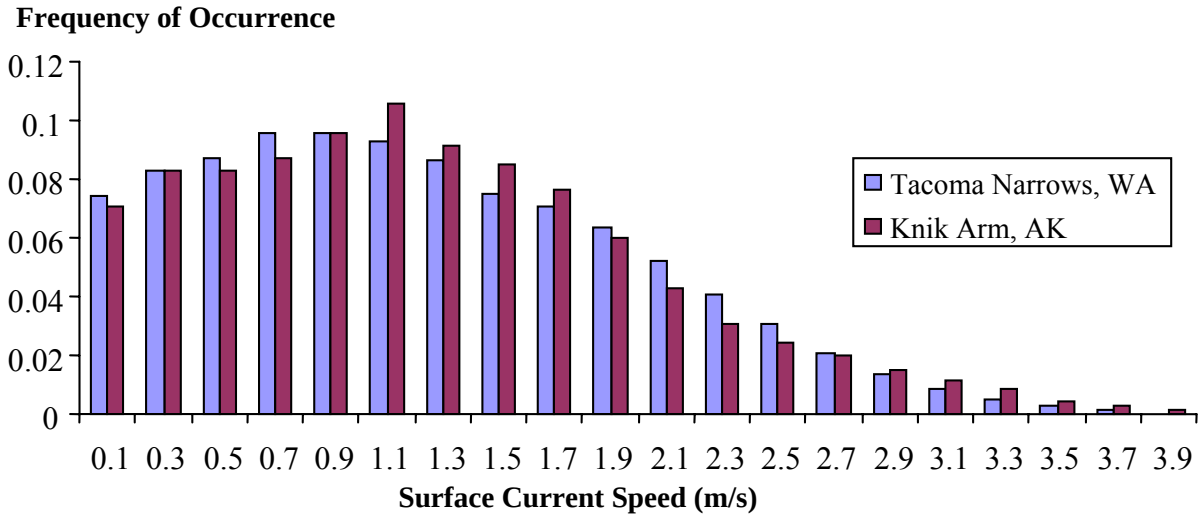

Figure 4-2. Surface Tidal Current Speed Probability Distributions for North American West Coast Sites

4.1.1. Sinusoidal Fit of Velocity Time History to Tidal Current Table Data

As detailed in Sections 2.1.2 and 2.1.5, tidal current tables list the day-by-day times of slack water and peak flows, and indicate the speed of those peak flows. This section describes the methodology developed by EPRI to construct a time history of 30-minute average velocities for Washington and Alaska by fitting a series of sinusoidal curve segments to such data. Current velocity is assumed to follows a sinusoidal time history, passing through each ebb or flood current peak between slack waters, as shown in Figure 4-3, below.

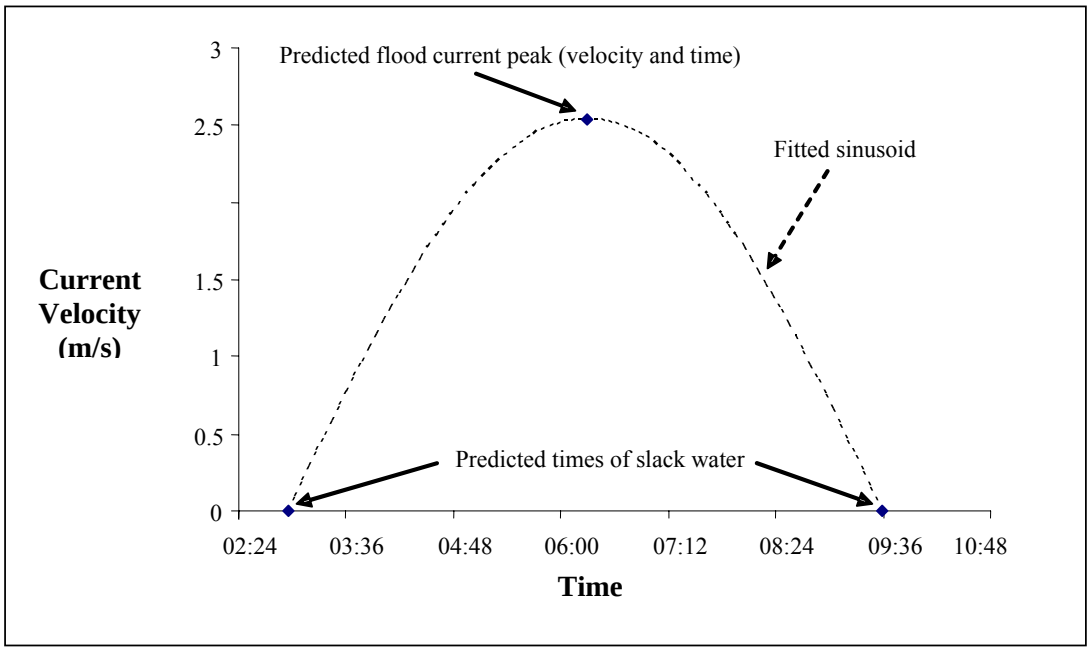

Figure 4-3. Sinusoidal Fit to Tidal Current Table Data

An idealized, sinusoidally varying current can be described by:

$$u(t) = U_{\max} \sin\left(\frac{\pi t}{T}\right)$$

where U_{max} is the predicted ebb or flood peak velocity, T is the period of oscillation, and $u(t)$ is the velocity at some time t during the oscillation. Since the peak ebb or flood currents often do not occur exactly between the two bracketing slack-water events, the half-sinusoid is broken up into two segments, one rising segment from slack to peak, and a second falling segment from peak to slack. The periods of these two curve segments are given by

$$T_{Rise} = \left(t_{\max} - t_{slack,1}\right) * 2$$
$$T_{Fall} = \left(t_{slack,2} - t_{\max}\right) * 2$$

Knowing the form of the velocity curve, the average of the velocity over a time interval ($t_2 - t_1$) may be calculated by:

$$\bar{u} = \frac{\int_{t_1}^{t_2} u(t)dt}{\int_{t_1}^{t_2} dt} = \frac{\int_{t_1}^{t_2} U_{\max} \sin\left(\frac{\pi t}{T}\right)dt}{\int_{t_1}^{t_2} dt} = \frac{-U_{\max}\frac{T}{\pi}\left(\cos\left(\frac{\pi t_2}{T}\right) - \cos\left(\frac{\pi t_1}{T}\right)\right)}{t_2 - t_1}$$

where t_1 is the start of the time interval and t_2 is the end of the averaging time interval.

For the time intervals of interest, the start and end time fall into one of four cases:

1. Velocity rising over entire time interval
2. Velocity falling over entire interval
3. Interval brackets a peak current event
4. Interval brackets a slack water event

For cases 1 and 2, the calculation procedure is to simply apply the equations for average velocity and power. For cases 3 and 4, averages are calculated for each of the two affected curve segments and the results combined in a weighted average.

The above procedure was programmed into an Excel workbook and used to incrementally calculate 30-minute average velocities as shown in Figure 4-4. In this manner, year-long time histories were constructed for surface currents at the design sites in Alaska and Washington.

For Knik Arm, AK, the prediction station used was “Cairn Point, northwest of (east side)” (61.267°N, 149.990°W, Station ID 4671). For Tacoma Narrows, WA, the prediction station used was “Point Evans, 0.1 mile east of” (47.286°N, 122.544°W, Station ID 1771).

Table Data

Day	Slack Water Time h.m.	Maximum Current Time h.m.	Maximum Current Velocity knots	Slack Water Time h.m.	Maximum Current Time h.m.	Maximum Current Velocity knots	Slack Water Time h.m.	Maximum Current Time h.m.	Maximum Current Velocity knots	Slack Water Time h.m.	Maximum Current Time h.m.	Maximum Current Velocity knots	Slack Water Time h.m.
1	245	559	2.1	916	1246	-2.2		1826	0.2		2358	-1.9	
2	327	636	1.8	941	1325	-2.3	1758	1930	0.4	2106			
3		58	-1.6	416	717	1.4	1007	1408	-2.6	1834	2038	0.7	2254
4		210	-1.2	517	803	0.9	1034	1453	-2.8	1912	2145	1.2	
5	40	332	-1.1	631	856	0.8	1105	1542	-3.1	1953	2248	1.7	
6	210	451	-1.1	655	955	0.6	1143	1633	-3.4	2036	2345	2.3	
7	322	601	-1.3	912	1053	0.5	1230	1725	-3.7	2122			
8		38	2.8	420	701	-1.5	1019	1155	0.5	1325	1817	-4.0	2209
9		128	3.2	510	754	-1.8	1[illegible]	1553	0.6	1424	1909	-4.2	2256
10		215	3.5	558	843	-2.1	1208	1549	0.7	1525	2000	-4.2	2343
11		302	3.6	638	930	-2.3	1259	1445	0.8	1627	2051	-4.1	
12	0	347	3.6	718	1017	-2.6	1350	1541	0.9	1729	2142	-3.8	
13	117	431	3.4	756	1103	-2.8	1444	1639	1.0	1833	2234	-3.4	
14	154	516	3.0	832	1150	-2.9	1539	1740	1.0	1942	2324	-2.8	
15	253	600	2.5	906	1237	-3.0	1636	1844	1.1	2059			
16		29	-2.2	345	645	2.0	939	1327	-3.1	1734	1954	1.2	2226
17		137	-1.6	444	733	1.5	1011	1418	-3.1	1838	2106	1.5	
18	2	254	-1.2	555	826	1.0	1042	1511	-3.1	1926	2216	1.6	
19	135	417	-1.1	721	924	0.6	1115	1605	-3.1	2017	2319	1.8	
20	252	534	-1.1	853	1026	0.3	1151	1658	-3.1	2104			
21		13	2.1	350	637	-1.2		1125	0.2		1747	-3.2	2146
22		100	2.3	437	727	-1.4		1218	0.2		1832	-3.2	2225
23		140	2.4	515	809	-1.6		1306	0.2		1912	-3.2	2301
24		216	2.6	548	845	-1.8	1233	1348	0.3	1500	1950	-3.2	2335
25		249	2.6	618	918	-1.9	1307	1427	0.4	1545	2025	-3.2	
26	7	320	2.6	646	949	-2.0	1339	1505	0.4	1629	2100	-3.1	
27	38	350	2.5	711	1019	-2.2	1411	1543	0.5	1714	2135	-2.9	
28	110	419	2.4	744	1049	-2.3	1443	1623	0.6	1803	2212	-2.6	
29	143	448	2.2	756	1119	-2.4	1516	1706	0.7	1858	2252	-2.3	
30	218	518	1.9	816	1151	-2.6	1553	1755	0.8	2002	2338	-1.9	
31	258	551	1.6	837	1227	-2.7	1634	1850	1.0	2116			

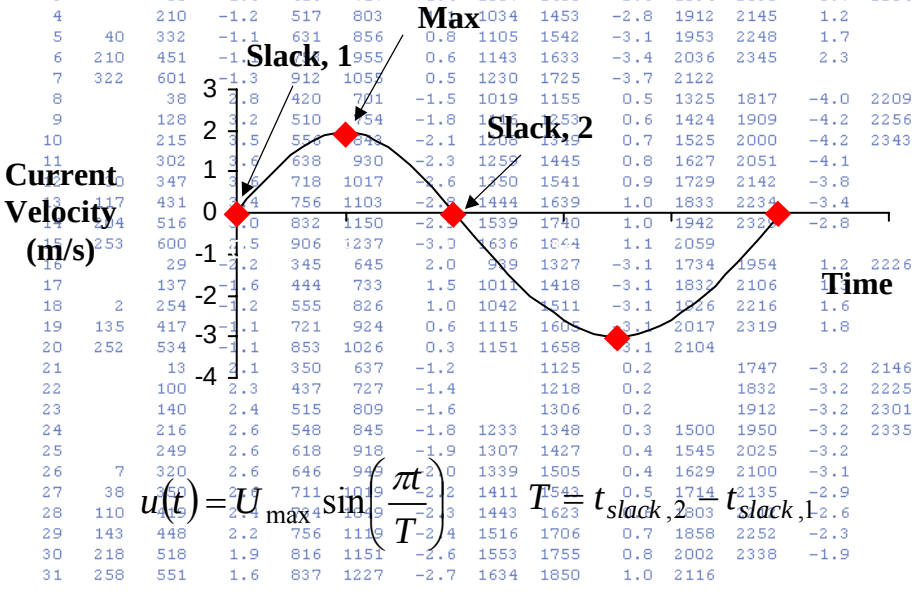

Time History

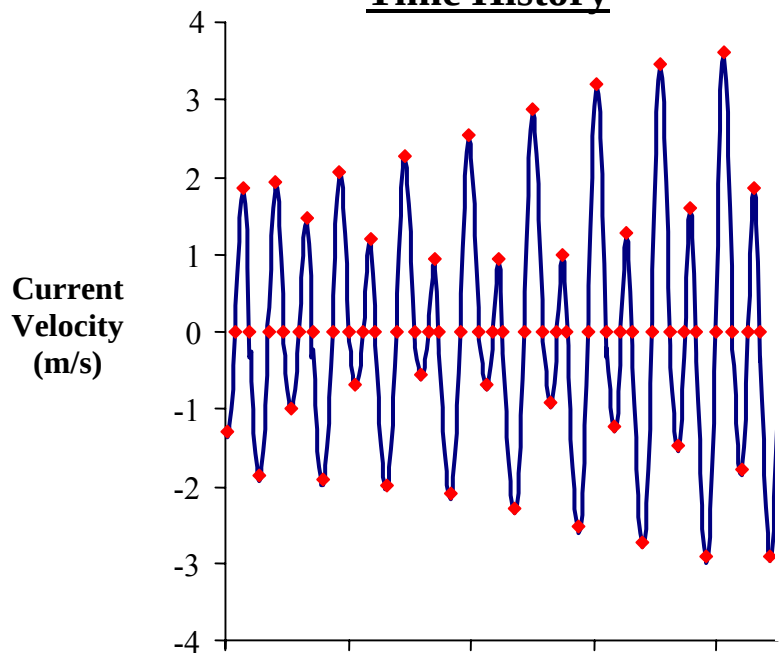

Figure 4-4. Construction of Velocity Time History

4.1.2. Extrapolation of Velocity Time History to a Different Channel Section

In San Francisco and Maine, the potential TISEC project sites are at narrow transects where the channel flow is most constricted and the tidal currents are fastest, but the NOS prediction stations are at wider transects where the currents are slower. For these two designs, open-channel flow theory was used to extrapolate predicted current speeds from the wider transect to the narrower transect where the project is located. Note that this does not account for the three-dimensional flow structure. For example, strong tidal flows often continue into a section of channel that is wider, manifesting as something akin to a "jet" of strong flow confined to the deeper, central channel, and not uniformly spreading out across its full width.

Because the tidal stream flow varies slowly with time and is sub-critical (Froude number <1), two open-channel fundamental equations can be applied to make this extrapolation. The first invokes continuity (conservation of mass), and the second invokes conservation of energy.

Continuity implies that mass is neither created nor destroyed. The governing relation states that in the absence of fluid inputs or outputs between two channel transects (e.g., no fresh water inputs from rivers or no drainage to other tributaries), then there is no change of fluid mass in the channel reach between the two transects, and the volumetric flow rate (Q, in cubic meters per second) remains constant. This equals the depth-averaged velocity (U, in meters per second) at a transect times the flow cross-sectional area (A, in square meters, which is equal to the depth of the flow, h, times the width of the transect, W):

$$Q = UA, \text{ where } A = hW$$

Conservation of energy in open-channel flow is expressed by the Bernoulli equation, which is best understood by referring to the accompanying definition sketch, below.

$$\left(z_1 + h_1 + \frac{U_1^2}{2g} \right) = \left(z_2 + h_2 + \frac{U_2^2}{2g} \right) + h_f$$

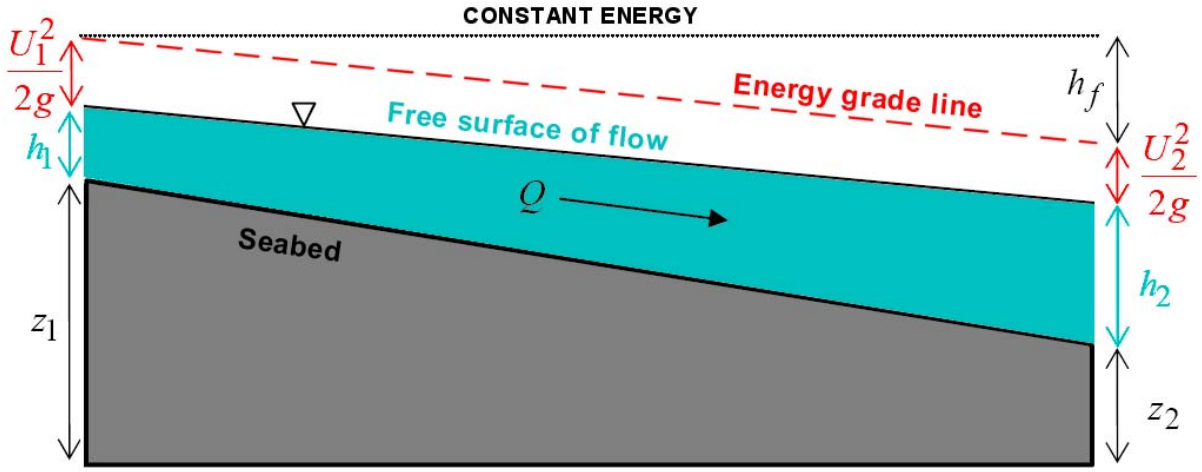

Figure 4-5. Open-Channel Flow Theory: Energy Equation and Definition Sketch

Assuming negligible friction loss (h_f) between the two transects, and if the seabed elevation and channel width are known at both locations, and if the flow depth and depth-averaged velocity are known at one transect (h_1 and U_1), then the unknown flow depth and depth-averaged velocity at the second transect (h_2 and U_2) can be found, because there are two equations (continuity of mass and conservation of energy) and two unknowns.

Writing the open-channel energy equation, neglecting the friction loss term:

$$z_1 + h_1 + \frac{U_1^2}{2g} = z_2 + h_2 + \frac{U_2^2}{2g}$$

Writing the continuity of mass equation in terms of channel width and depth:

$$W_1 h_1 U_1 = W_2 h_2 U_2$$

and re-arranging to state h_2 in terms of U_2:

$$h_2 = W_1 h_1 U_1 / W_2 U_2$$

and then substituting this expression for h_2 in the energy equation above yields an equation with two real roots, only one of which matches the known flow conditions at Transect 1. An example problem and solution is given below.

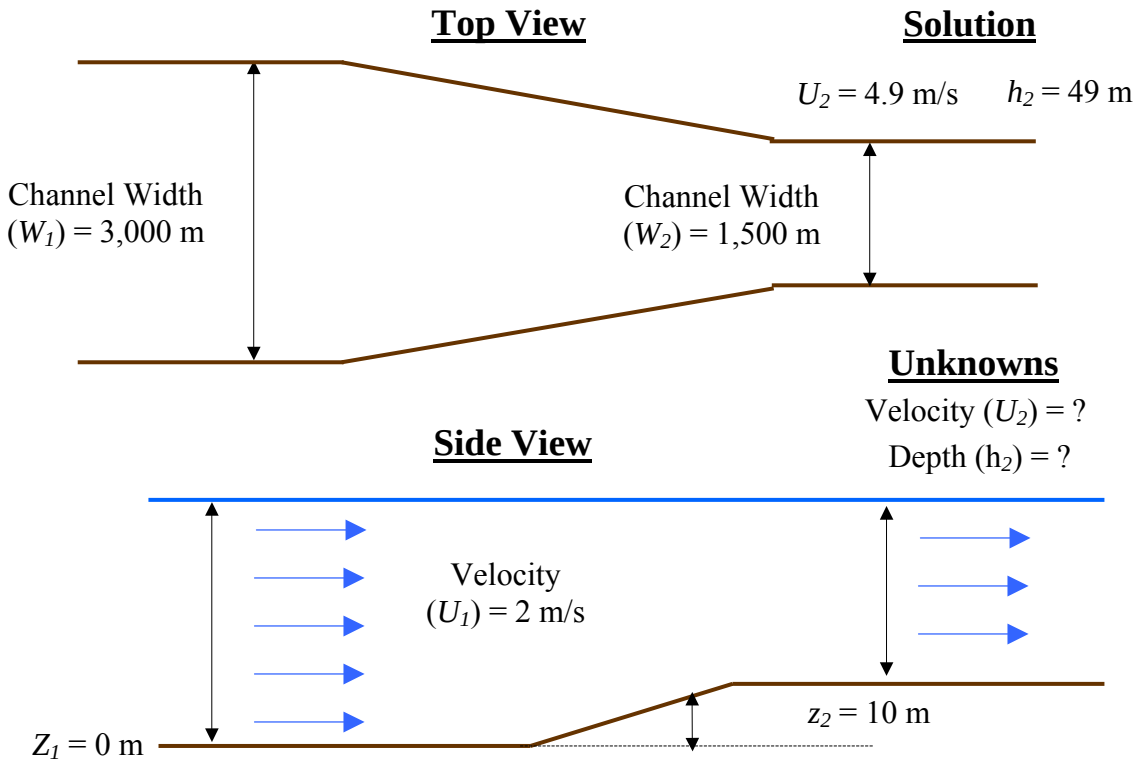

Figure 4-6. Example Application of Open-Channel Flow Theory

4.1.3. *WebTide* Velocity Time History for Head Harbour Passage, NB

Fourteen figures (4-7 through 4-20)

(Reference 9)

(Reference 10)

4.1.4. *WebTide* Velocity Time History for Minas Passage, NS

WebTide Velocity Time History for Minas Passage, NS

Eight figures (4-21 through 4-28)

(Reference 10)

4.2. Turbine Hub-Height Current Velocity Distribution

As mentioned earlier, navigation clearance requirements will necessitate the submergence of a tidal stream turbine sufficient to have at least a 5-m clearance for shallow-draft vessels, and possibly 15-20 m of clearance in channels traversed by oceangoing vessels. This means that once the surface velocity time history (and thus probability distribution) is known, it must be adjusted to account for turbine depth below the sea surface.

Surface velocities must be adjusted to determine the velocity and power density averaged over the circular area swept by the turbine rotor, centered at the turbine hub height. As explained below, this can be approximated to within a few percent by simply taking the power density at hub height as being representative of the power density over the entire rotor.

As before, the vertical velocity profile for the channel is approximated by a $1/10^{th}$ power law.

$$u_{hub} = u_{surface}\left(\frac{z_{hub}}{z_{surface}}\right)^{1/10}$$

where u_{hub} is the velocity at hub height, $u_{surface}$ is the surface velocity, z_{hub} is the elevation of the hub above the seafloor, and z_{hub} is the depth of the channel.

More rigorously, the average power over the swept area of the rotor is exactly given by:

$$\overline{P} = \frac{\int_0^{2\pi}\int_0^{R} \frac{1}{2}\rho u_{surface}^3 \left(\frac{r\sin\theta + z_{hub}}{z_{surface}}\right)^{3/10} r\,dr\,d\theta}{\int_0^{2\pi}\int_0^{R} r\,dr\,d\theta}$$

where R is the radius of the rotor and z_{hub}, $z_{surface}$, and $u_{surface}$ are as defined previously. This integral is not readily evaluated by analytical methods, but may be approached numerically. This is done by approximating the rotor as a series of rectangles with height Δz and width Δx. The power density for each rectangular area is calculated, and an area-weighted average taken to find the average power density over the rotor.

The variance between the hub-height approximation and the exact integration method is plotted in Figure 4-29. Note that this variance is independent of channel depth and flow velocity, but it does depend on the ratio of turbine radius to hub height. For the extreme case of a ratio of unity (turbine blade tip just touches seabed at bottom of rotation) the approximation error is just under 4%. For more realistic cases, such as those in the feasibility study, the approximation error is less than 1%. It should be noted that in all cases, the approximation error is negative – that is, the approximation under-predicts turbine power, and our results are conservative.

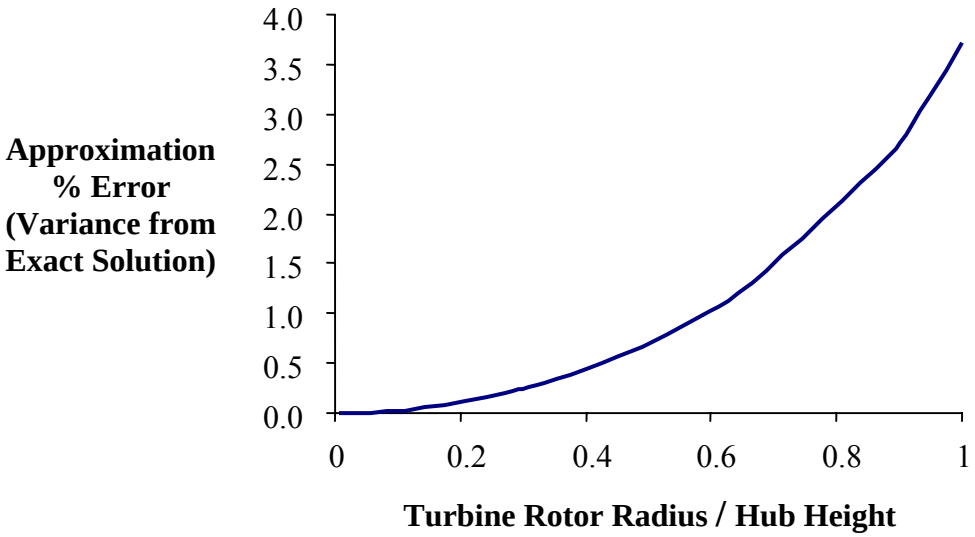

Figure 4-29. Incident Flow Power Error for Hub-Height Approximation

If the surface velocity time history has been sorted into a velocity probability distribution, then the surface speed bin categories can be adjusted to represent hub-height speeds, as shown below.

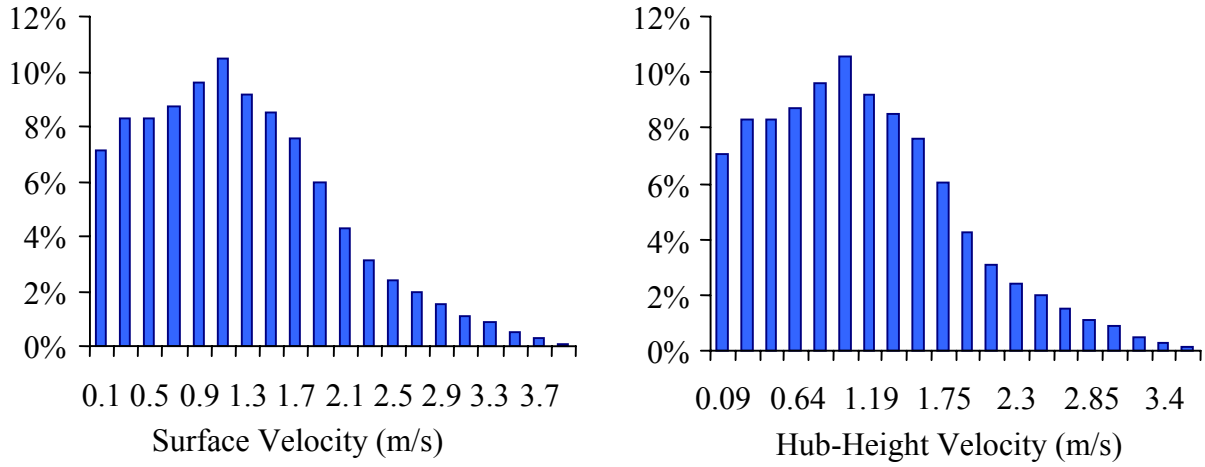

Figure 4-30. Depth Adjustment of Velocity Bins in Probability Distribution

Alternatively, the depth adjustment can be applied at each time step for which the surface current velocity is known, to calculate the 30-minute average velocity across the depth span of the rotor swept area. Either method uses the same hub-height depth correction multiplier, calculated as described above.

4.3. Electric Power Output

Once the surface velocities have been adjusted to hub-height and averaged across the depth span of the rotor swept area, each current speed value is tested for one of three conditions (refer back to Figure 1-10), and the output estimated as follows:

I. Velocity below cut-in speed.
   No power generated.

II. Velocity between cut-in speed and rated speed.
   Electric power output calculated according to the following equations

$$P_{\text{Delivered Electric}} = A_{\text{Turbine}} \times \left(\frac{P}{A}\right)_{\text{Water}} \times \eta_{\text{TFC}}$$

where $\eta_{\text{TFC}} = \eta_{\text{Turbine}} \times \eta_{\text{Drive Train}} \times \eta_{\text{Generator}} \times \eta_{\text{Power Conditioning}}$

For variable-pitch rotors, η_{Turbine} can be assumed to be constant, but the other component efficiencies vary with percentage load (defined as extracted power divided by rated power x 100).

III. Velocity exceeds rated speed.
   Electric power = rated capacity

The above calculation is carried out for each time increment with the results averaged over the full course of the time history to find the average turbine output power. For example, with a year-long time history of 30-minute average velocities, there would be 17,520 resulting data points for 30-minute average power output. Summing these over the course of the year and then dividing by 17,520 would yield the annual average power output.

Alternatively, the above calculation can be carried out on each bin of the velocity distribution profile, with the resulting power output multiplied by the fraction of time each bin occurs during a year and the results summed across all bins. Provided that the speed bins have sufficiently high resolution (0.2 m/s increments yield the smallest discretization error), then this approach will give results that closely agree with the time history approach.

Using the time history approach has the advantage of being able to see how power output varies over different averaging periods. Examples from the Tacoma, Washington site at Point Evans are given in Figures 4-31 through 4-35. Note how diurnal inequality substantially reduces array capacity factor in Figure 4-33.

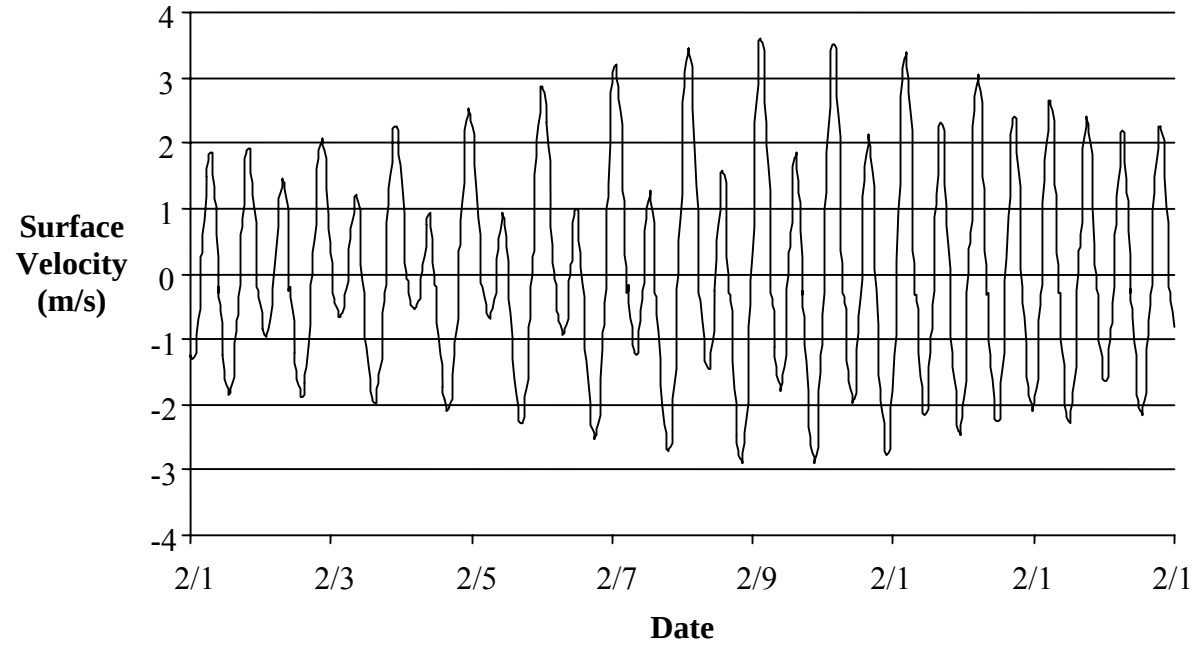

Figure 4-31. Tidal Stream Velocity Variation at Point Evans (01-14 Feb 2005)

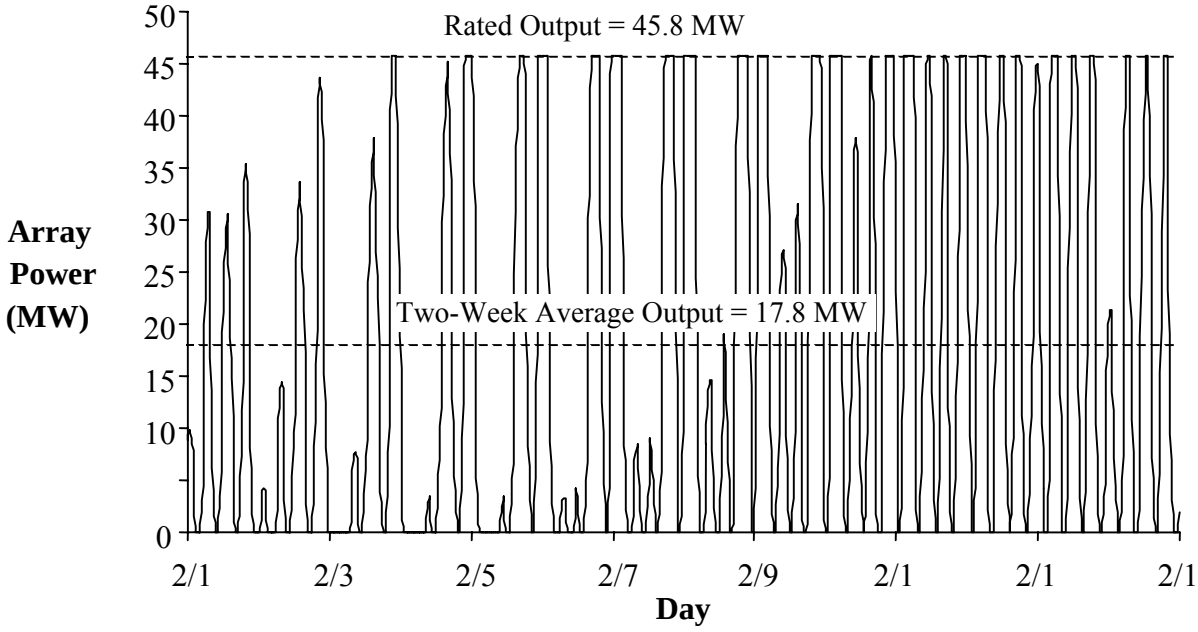

Figure 4-32. Array Output Variation at Point Evans (01-14 Feb 2005)

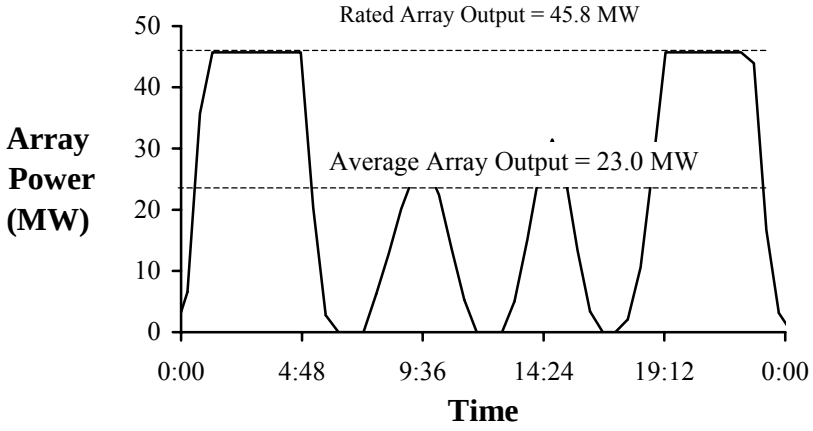

Figure 4-33. Array Output 30-Minute Averages at Point Evans (09 Feb 2005)

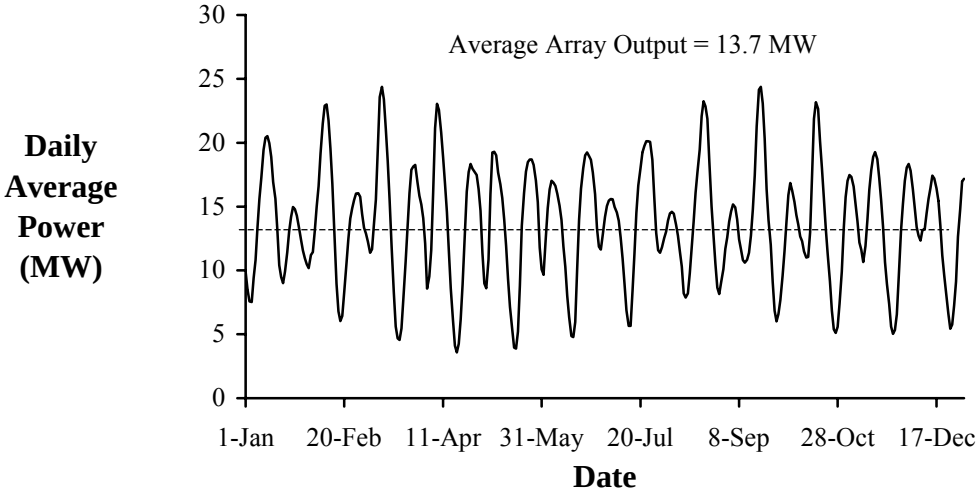

Figure 4-34. Array Output Daily Averages at Point Evans (01-14 Feb 2005)

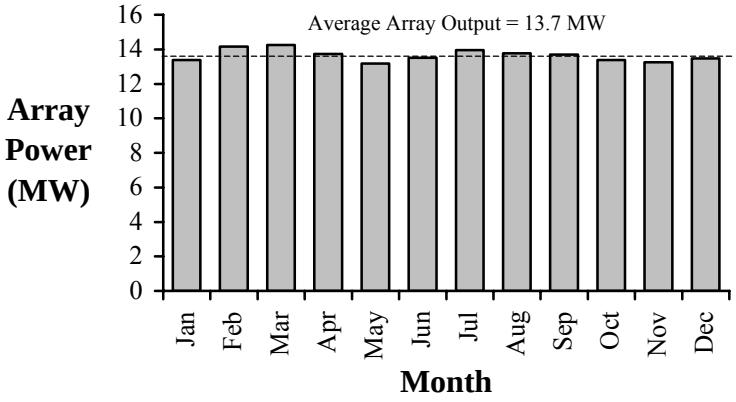

Figure 4-35. Array Output Monthly Averages at Point Evans (2005)

4.4. Annual Energy Production

Once the turbine electric power output has been determined, turbine energy production may be obtained by multiplying the annual average power output by 8,760 hours per year to obtain the maximum possible annual electrical energy production, assuming that the turbine is available 100% of the time.

In reality, scheduled outages for routine inspection and maintenance, as well as forced outages for repair, will reduce the percentage of time that the turbine is available to generate power. For this Phase 1 feasibility study, EPRI assumed an availability of 95% (consistent with Reference 11). The TP-006 Design Reports include availability as one of the parameters for which cost-of-energy sensitivity studies were performed. Since the grid interconnection was designed for a 2% line loss, array output was further multiplied by 98% transmission efficiency.

4.5. Maximum Project Size

The maximum project size governs the possible economies of scale and the number of turbines that can be installed at a site, which can strongly influence the cost of energy (see 006 Design Reports for sensitivity analysis of this parameter). The commercial project sizing approach used for the EPRI Phase 1 conceptual designs was to first establish the total size of the physically available resource, then estimate the environmentally constrained extraction limit based on the percentage of the available resource that can be extracted with negligible environmental impact on the surrounding environment, and finally to determine if the depth, width, and length of the channel constrained the number of turbines short of reaching the environmental extraction limit.

Thus the size of the project was determined to be the lesser of these two variables: the maximum number of turbines withdrawing the environmental extraction limit, or the maximum number of turbines that could be physically placed in the channel.

4.5.1. Influence of Tidal Range on Physical Resource Estimates

The environmental extraction limit is stated as a percentage of the available physical resource (annual average tidal stream power across entire channel cross-section). In turn, the size of the available physical resource is a product of the mean annual, depth-averaged tidal stream power density and the cross-sectional area of the channel.

Section 3.2 describes how mean annual power density was estimated for the site surveys in MA, ME, NB, and NS. This same procedure was used to estimate mean annual power density for the commercial project size estimate at the selected sites in those four states and provinces, as well as for the three sites on the west coast: AK, WA, and San Francisco.

Likewise, Section 3.3 describes how channel cross-sectional area was estimated for the east coast sites, whereby the channel's subtidal cross-sectional area was added to a rectangular area whose width is the distance between the MLLW shorelines, and whose height is equal to half the mean tidal range. This simplified procedure was used for the commercial project size estimate at the four east coast sites and San Francisco. This is a reasonable approximation for those sites, where tidal range is small relative to MLLW depth, and where the shoreline is relatively steep, without extensive shoals that have substantial tidal flow over them at high tide, even though they may be shallow and quiescent or even dry out at low tide.

For the sites in AK and WA, a considerably more sophisticated procedure was used, which takes into account the co-variant nature of tidal stream power density and channel cross-sectional area. The first step in this procedure was to develop a digital bathymetric map for accurate transect elevation estimates across the width of the channel. This procedure is described in Appendix B.

Since the spacing of grid points from the digital bathymetric map is uniform along the transect, they simply can be averaged to find the mean channel depth relative to MLLW. This is then multiplied by the channel width (distance between outermost transect end points that have negative elevations) to find the cross-sectional area below MLLW, which is referred to as the baseline area.

The third step was to locate the NOAA tide prediction station (for tidal water level changes) closest to the tidal current reference site and produce a coincident time-history for the height of water level above or below MLLW, in 30-minute increments. Note that tide levels below MLLW must be made positive, so that when added to the baseline depth (which is a negative number), the new depth becomes less negative (shallower). Likewise, tide levels above MLLW must be made negative, so that when added to the baseline depth, the new depth becomes more negative (deeper). This yields a time-history of channel cross-sectional area.

The final step is to synchronize and step through the two time histories, one of depth-averaged power density, and one of channel cross-sectional area, and multiply the two at each time step, which yields a time history of total tidal stream power. Averaging the results over the course of a year yields the mean annual power.

By comparison with the simplified approach described in Section 3.3, this can yield a significant increase in the estimated size of the physical resource. This is because it includes current flows over shoal areas as they become deeper on a rising tide. It should be noted, however, that the above procedure assumes that the depth-averaged tidal stream power density applies uniformly across the width of the channel, but this is unlikely to be true. It does provide, however, an upper bound to the expected increase in the estimated size of the physical resource if the coincident nature of changing tidal water levels and changing tidal current speeds was properly modeled. This in turn would indicate whether or not it would be warranted to undertake an even more sophisticated approach that would involve full three-dimensional finite element modeling of both water levels and currents in the channel.

4.5.2. Energy Extraction Constraints

Given the similarities between wind turbines and tidal stream turbines, it is tempting to believe that with sufficient downstream spacing to avoid wake effects, an unlimited number of turbine rows can be placed along the length of a tidal channel. The basic nature of the tidal stream and wind energy resources is quite different, however, as explained below.

Wind turbines extract energy from the lower turbulent boundary layer of the atmosphere, and as energy is extracted this reduces the wind speed immediately behind the turbine and increases the rate of downward turbulent momentum transfer until the wind speed essentially re-establishes itself a relatively short distance downwind of the turbine. Wind energy is thus replenished from above, drawing from airflows extending the full height of the troposphere, which is 16-18 km thick over the equator and about 10 km thick over the poles.

In contrast to atmospheric flows, tidal stream flows are constrained between the seabed and sea surface, in depths that are usually less than 100 m. Tidal stream energy is therefore more spatially constrained, and withdrawal of excessive amounts could reduce natural circulation to the point that significant environmental effects occur.

Only a few studies have been published that address this subject. In a review of tidal stream resource assessments for the Carbon Trust, Black & Veatch Consulting, Ltd., has adopted a 20% "Significant Impact Factor" as the percentage of the total available resource that can be extracted without significant environmental effect (Reference 11).

Early numerical modeling by Ian Bryden and his colleagues led them to suggest 10% as a "rule of thumb" conservative estimate of the extractable resource in a simple channel (Reference 12). This was based on the application of open-channel flow theory to simulate a tidal channel connecting two unconstrained bodies of water (as between two islands, for example). The modeled tidal channel had a width of 1 km, a length of 4 km, and a natural tide level difference of 0.8 m between each end of the channel. Results are shown below.

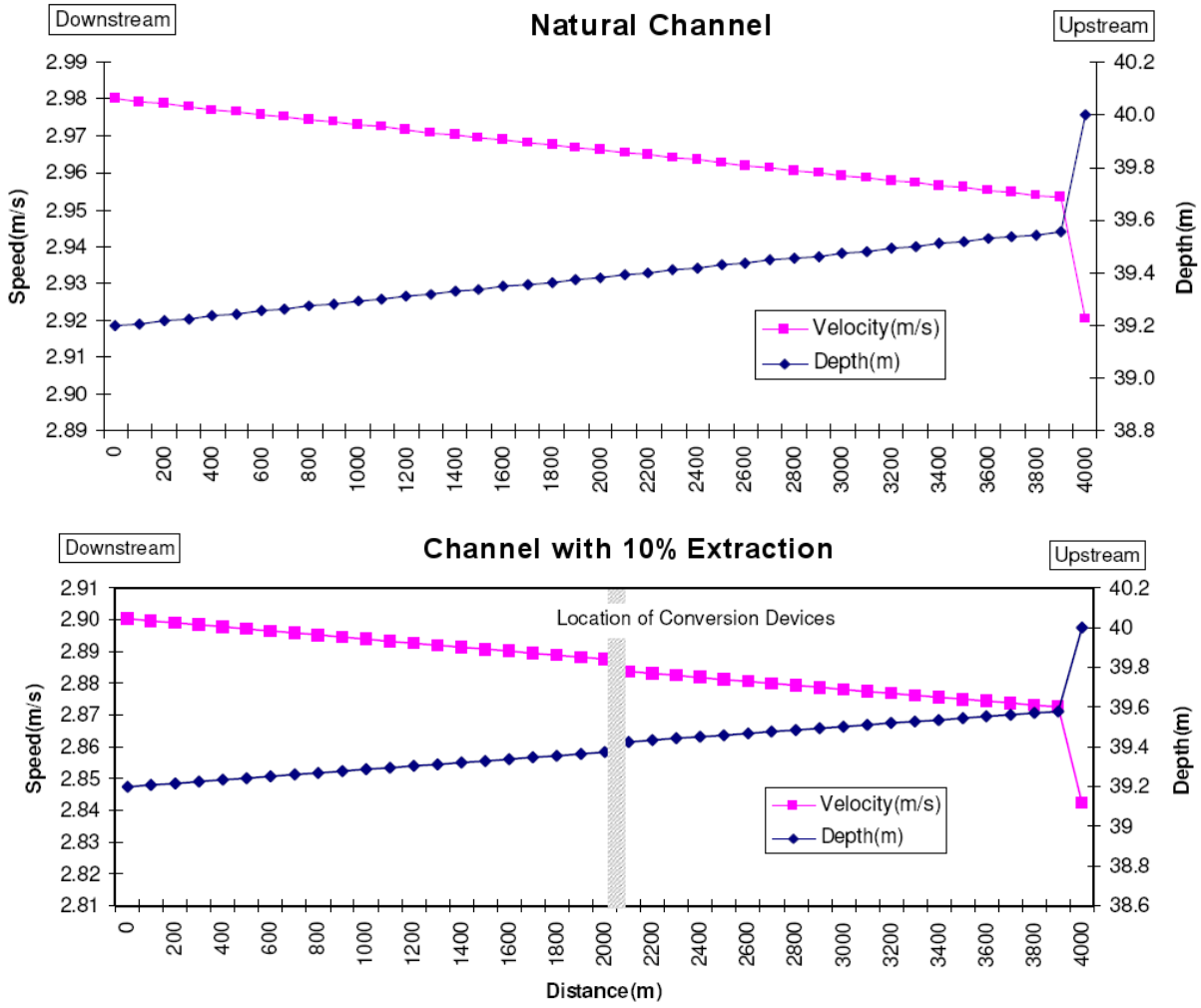

Figure 4-36. Influence of Energy Extraction on Flow in a Tidal Channel

Note the localized steepening of the water surface gradient in the immediate vicinity of the turbine array, which creates a localized jump in flow speed. This locally increases the kinetic energy flux such that the 10% notional extraction level actually corresponds to a 9.2% drop in kinetic energy flux compared to the natural channel. The overall reduction in flow speed along the entire channel length averages 2.6%.

A subsequent paper (Reference 13) extends this analysis to a sea loch inlet, where an enclosed basin area of 50 km^2 communicates to an unconstrained ocean by a channel that is 500 m long, 200 m wide, and 30 m deep. It was noted that as with the straight channel, flow blockage and energy extraction by the turbine array creates a locally steep sea surface gradient, as the rate of tidal loch filling or emptying decreases when the channel is blocked by a row of turbines. In this particular case, the authors suggest that up to 30% of the natural flux may be extractable.

In reviewing these results, EPRI has used 15% as the environmental extraction limit. According to the open-ended channel model results reported in Reference 13, this would result in a tidal current speed reduction averaging 4% along the entire channel length. It is unknown whether or not such a change in flow speed would result in significant environmental consequences, such as slower transport of nutrients and oxygen or less turbulent mixing. Also, the above results were for very simple channel geometries in simplified flows. Better understanding of these effects would require the development of ecosystem-level models, driven by site-specific hydrodynamic numerical models, reflecting actual site bathymetry and tidal changes in sea level, as well as turbine-specific interactions with the flow.

It also is important to note that the above percentages are based on numerical modeling only, and that these results have not been verified by physical experiments. Therefore, not only are more sophisticated numerical models required, but also they must be validated with appropriately scaled physical models in laboratory current flumes.

The total power in a tidal stream is the summation of the kinetic energy due to its velocity and the potential energy due to its height. In order to satisfy both conservation of mass and energy, after each transect, the height of the water decreases and velocity increases. The net effect is a decrease in total channel power, but an increase in the downstream kinetic energy component, as steeper sea level gradients drive increased flow speeds. This effect is described for an ideal channel in a recent paper by Bryden and Couch (Reference 13). If this can be verified by laboratory experiments, then this could greatly increase the potential maximum project size.

4.5.3. Turbine Spacing and Physical Placement Constraints

In order to estimate the number of turbines that could be placed in the seabed "footprint" area that is within the appropriate depth regime for a particular type of tidal stream turbine, the following turbine spacing was assumed for conceptual design lay-out:

- Across-channel: 1/2 diameter gap between adjacent turbine rotors within row
- Along-channel: 10 diameter separation between adjacent rows of turbines

These turbine spacing arrangements are based on analogues to wind turbine spacing and should be verified by numerical and physical modeling during the next project phase.

It should be noted that Myers and Bahaj (Reference 15) use a 3-diameter gap between adjacent turbine rotors within row and an along-channel spacing of 15 rotor diameters. Their results indicate a substantial reduction in tidal stream velocity from row to row, and degraded array performance for arrays with more than a few rows of turbines.

Their analysis appears to violate the conservation of mass law for open channels by assuming a constant cross-sectional flow area. If the flow speed decreases from turbine row to turbine row, however, then the depth of the flow must increase to maintain conservation of mass. This is in direct contrast to the numerical modeling results of Bryden and his colleagues reviewed above, where flow speeds actually increase in the local vicinity of the turbine row, and there is a local decrease in the depth of flow.

4.5.4. Number of Homes Powered

In order that one may easily relate the average annual extractable power number for a tidal plant to something that most people have a feel for, we use the number of U.S. homes that can be powered by that plant. From the International Energy Agency, we know that, in 2003, the average power used by a U.S. residence was 1.3 kW. Therefore number of homes powered is equal to the average annual extractable power of the tidal current stream (15% of the total mean annual resource) times the efficiency of generating electricity from the extracted energy divided by 1.3 kW per average U.S. home.

The drive train, generator, and power conditioning component efficiencies values (i.e., the total efficiency of generation electrical energy from extracted energy) used for this purpose were:

- $\eta_{\text{Drive Train}} = 96\%$
- $\eta_{\text{Generator}} = 95\%$
- $\eta_{\text{Power Conditioning}} = 98\%$

Multiplication of these component efficiencies yields an estimate of 90% for the extracted flow energy in the tidal stream that would be converted into electrical energy.

5. References

1. Boon, J., 2004. *SECRETS OF THE TIDE: Tide and Tidal Current Analysis and Predictions, Storm Surges and Sea Level Trends*. West Sussex, UK: Horwood Publishing, Ltd. 300 pp.

2. "Assessment of the National Ocean Service's Tidal Current Program". NOAA Technical Report NOS CO-OPS 022, April 1999.

3. Canadian Hydrographic Service, 2005. *Canadian Tide and Current Tables, Volume 1, Atlantic Coast and Bay of Fundy*. Ottawa: Fisheries and Oceans Canada, Cat. No. Fs 73-2005/1.

4. DeWolfe, D.L., Canadian Hydrographic Service, 1981. *Atlas of Tidal Currents, Bay of Fundy and Gulf of Maine*, P241. Ottawa: Fisheries and Oceans Canada.

5. Brooks, D.A., 2005. "The tidal-stream energy resource in Passamaquoddy-Cobscook bays: a fresh look at an old story," *Renewable Energy* (submitted for publication).

6. Brooks, D.A., 2005. "Mpower.avi Streaming power density, full Quoddy region." (http://cobscook.tamu.edu/review/).

7. U.S. National Oceanic and Atmospheric Administration, 2005. *Coast Pilot, 35th Edition*. (http://nauticalcharts.noaa.gov/nsd/cpdownload.htm).

8. Canadian Hydrographic Service, 2001. *Sailing Directions, Gulf of Maine and Bay of Fundy*. *ATL-106*. Ottawa: Fisheries and Oceans Canada, Cat. No. Fs 72-3/2001-6E.

9. Xu, D., H. Xue, D.A. Greenberg, 2006. A numerical study of the circulation and drifter trajectories in Cobscook Bay. *9th International Conference on Estuarine and Coastal Modeling* (submitted manuscript).

10. Cornett, A., 2006. *Inventory Of Canada's Marine Renewable Energy Resources* Canadian Hydraulics Centre (Report No. CHC-TR-041, April 2006). Ottawa: National Research Council

11. Black & Veatch Consulting, Ltd., 2004. "UK, Europe, and Global Tidal Energy Resource Assessment." Marine Energy Challenge Report No. 107799/D/2100/05/1. London: Carbon Trust.

12. Bryden, I.G., T. Grinsted, and G.T. Melville, 2004. Assessing the potential of a simple tidal channel to deliver useful energy. *Applied Ocean Research 26*: 198–204

13. Bryden, I.G., and G.T. Melville, 2004. Choosing and evaluating sites for tidal current development. *Proc. Instn. Mech. Engrs., Part A: Journal of Power and Energy*, *Vol. 218,* pp. 567-577.

14. Bryden, I.G., and S.J. Couch, 2006. ME1—marine energy extraction: tidal resource analysis. *Renewable Energy 31*: 133-139.

15. Myers, L., and A.S. Bahaj, 2005. Simulated electrical power potential harnessed by marine current turbine arrays in the Alderney Race. *Renewable Energy 30*: 1713-1731.

Appendix A

Fluid Flow Power Theory Applied to Wind and Tidal Stream Power Density Calculations

1. Air Flow

Because air has mass and it moves to form wind, it has ***kinetic energy***.

kinetic energy (joules) = 0.5 x m x V^2

where:
m = mass (kg) (1 kg = 2.2 pounds)
V = velocity (meters/second) (meter = 3.281 feet = 39.37 inches)

We are more interested in power (which changes moment to moment) than energy. Since **energy = power x time and density** is a more convenient way to express the mass of flowing air, the kinetic energy equation can be converted into a flow equation:

Power in the area swept by the wind turbine rotor:

$P = 0.5 \times \rho \times A \times V^3$

where:
P = power in watts (746 watts = 1 hp) (1,000 watts = 1 kilowatt)
ρ = air density (about 1.225 kg/m^3 at sea level, less higher up)
A = rotor swept area, exposed to the wind (m^2)
V = wind speed in meters/sec (20 mph = 9 m/s) (mph/2.24 = m/s)

This yields the power in a free flowing stream of wind. Of course, it is impossible to extract all the power from the wind because some flow must be maintained through the rotor. So, we need to include some additional terms to get a practical equation for a wind turbine.

Wind Turbine Power:

$P = 0.5 \times \rho \times A \times V^3 \times f_{Turbine} + f_{DriveTrain} + f_{Generator} + f_{PowerConditioning}$

where:
P = power in watts (746 watts = 1 hp) (1,000 watts = 1 kilowatt)
ρ = air density (1.225 kg/m^3 at sea level, less higher up)
A = rotor swept area, exposed to the wind (m^2)
V = wind speed in meters/sec (27 mph = 12 m/s)

$f_{Turbine}$ = Turbine Efficiency (0.59 {Betz limit} is the maximum theoretically possible, 0.47 for a very good design)
$f_{DriveTrain}$ = gearbox/bearings efficiency (depends, could be as high as 95% if good)
$f_{Generator}$ = generator efficiency (50% for car alternator, 90% or possibly more for a permanent magnet generator or grid-connected induction generator)
$f_{PowerConditioning}$ = Power conditioning efficiency (90%)

Therefore, wind power density in a 12 meter/sec (20 mph) wind is

$$P/A = \tfrac{1}{2} \times \rho \times V^3 = \tfrac{1}{2} \times 1.2 \times (12)^3 = 1.037 \ kW/m^2$$

Assuming a wind turbine rated at a velocity of 12 m/sec with a combined $f_{Turbine} + f_{DriveTrain} + f_{Generator} + f_{PowerConditioning} = 0.36$

$$\text{Delivered power density} = 1.037 \ kW/m^2 \times 0.36 = 0.37 \ kW/m^2$$

For a real case, the wind velocity scatter diagram (wind velocity versus hours of occurrence per year) is known and the wind turbine cut-in, power output vs wind speed input and cut-out velocities are known. Assuming the wind speed does not vary from its stated value across the plan form of the wind rotor, the yearly electrical output is easily calculated.

2. Water (Tidal, River and/or Current) Flow

Next, water flow power density at 3 m/sec is

$$P = \tfrac{1}{2} \times \rho \times V^3 = \tfrac{1}{2} \times 1000 \times (3)^3 = 13.5 \ kW/m^2$$

Assuming the same $f_{Turbine} + f_{DriveTrain} + f_{Generator} + f_{PowerConditioning} = 0.36$ then

$$\text{Delivered power density} = 13.5 \ kW/m^2 \times 0.36 = 4.9 \ kW/m^2$$

Therefore, the power density of tidal flow energy at a tidal flow current speed of 2 m/sec is about 9 times greater than that for wind energy at a speed of 9 m/sec.

Appendix B

Creation of Digitized Channel Cross-Sections from Soundings Data

Source of Data

Digital bathymetric data in the form of individual hydrographic soundings were accessed through a GIS web interface posted by the U.S. National Oceanic and Atmospheric Administration at http://map.ngdc.noaa.gov/website/mgg/nos_hydro/viewer.htm. Each sounding is in XYZ format (latitude, longitude, and depth). Bathymetric data for surveys over much of the 20th century are available - with sounding density increasing over time. Depth is referenced to Mean Lower Low Water (MLLW), the average of the lowest tides of each day in a Tidal Epoch. Negative numbers indicate soundings below MLLW, whereas positive numbers indicate elevations above MLLW. Example data for Knik Arm, which has extensive intertidal flats, are given in the table below.

Table B1. Representative XYZ Data

X (Longitude)	Y (Latitude)	Z (Depth - MLLW)
-150.284943	61.129938	0.6
-150.283488	61.130538	0.6
-150.281938	61.131049	0.3
-150.285507	61.131616	-0.3
-150.280899	61.131713	0.3
-150.285046	61.132063	0.3
-150.284716	61.132246	-0.3
-150.279793	61.132366	0.3
-150.296566	61.124638	-10.7

Creation of Digital Map

For a particular site all applicable data were downloaded from the above Web page and pasted into a spreadsheet. A macro then superimposed these data onto a grid using the Haversine formula. Macro inputs are the vertical (N-S) and horizontal (E-W) grid size and the bounding lines of latitude and longitude for the region of interest.

The Haversine formula (see http://en.wikipedia.org/wiki/Haversine_formula for derivation and http://www.movable-type.co.uk/scripts/LatLong.html for a wide variety of different applications) computes the linear distance between two points of latitude and longitude and is given by:

$$a = \sin^2\left(\frac{lat_1 - lat_2}{2}\right) + \cos(lat_1)\cos(lat_2)\sin^2\left(\frac{lon_1 - lon_2}{2}\right) \qquad \text{(Equation B1)}$$

where lat_1,lon_1 are the latitude and longitude in radians of the first point and lat_2,lon_2 are for the second point.

The great circle distance, in radians, between the two points, *c*, is given as:

$$c = 2\tan^{-1}\left(\frac{a^{1/2}}{(1-a)^{1/2}}\right) \qquad \text{(Equation B2)}$$

where *a* is calculated using (Equation 1). The value for c can be converted to a metric distance, d, using the radius of the earth (r = 6,378,135m):

$$d = Rc \qquad \text{(Equation B3)}$$

To create the digital bathymetric map, the N-S and E-W distances from a fixed reference (the minimum latitude and longitude bounding the region of interest; see Figure B1) are calculated.

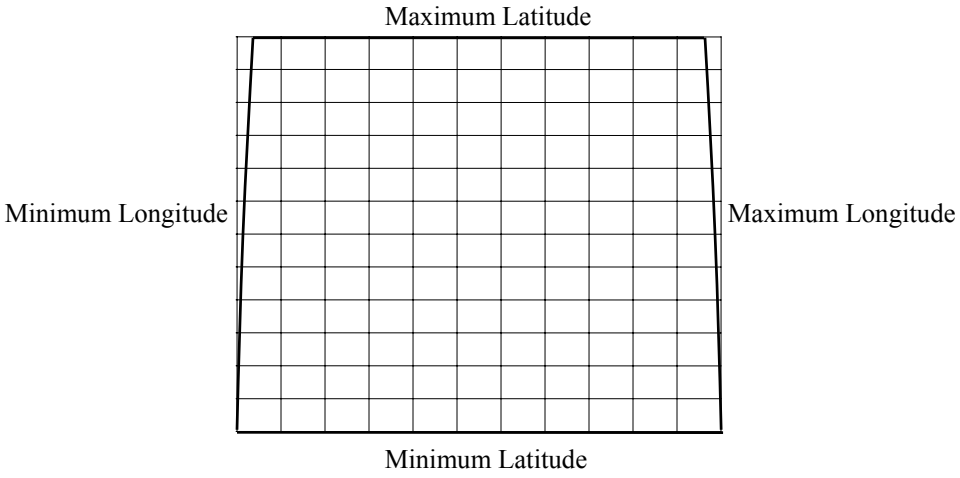

Figure B-1. Digital Grid Superimposed on Region of Interest

The N-S (vertical on spreadsheet) distance is given by:

$$d_{N-S} = \sin^2\left(\frac{lat_1 - lat_2}{2}\right) \qquad \text{(Equation B4)}$$

Due to the curvature of the earth, calculating the E-W (horizontal on spreadsheet) distance from the reference must be carried out in two steps. First, the great-circle distance, *d*, between the reference and point of interest is calculated using Equations B1 through B3. Then, the following equation is used with the previously calculated N-S distance to find the E-W distance as:

$$d_{E-W} = \left(d^2 - d_{N-S}\right)^{1/2} \qquad \text{(Equation B5)}$$

Once the N-S and E-W distances have been determined, the grid the latitude and longitude fall into is found by dividing the distance by grid size (horizontal or vertical). If multiple data points fall into the same grid element, they are averaged to give an average depth for the grid element.

Excessively wide grid spacing results in too much averaging, whereas excessively narrow grid spacing results in blanks where no survey data is available. A grid spacing of 120m on edge appears optimal for Tacoma Narrows hydrographic data. Sample output from this site is shown in Figure B-2. The grid color coded to show viable turbine sites (red = too shallow, blue = too deep, green = valid site). White blocks without data indicate gaps in the hydrographic survey.

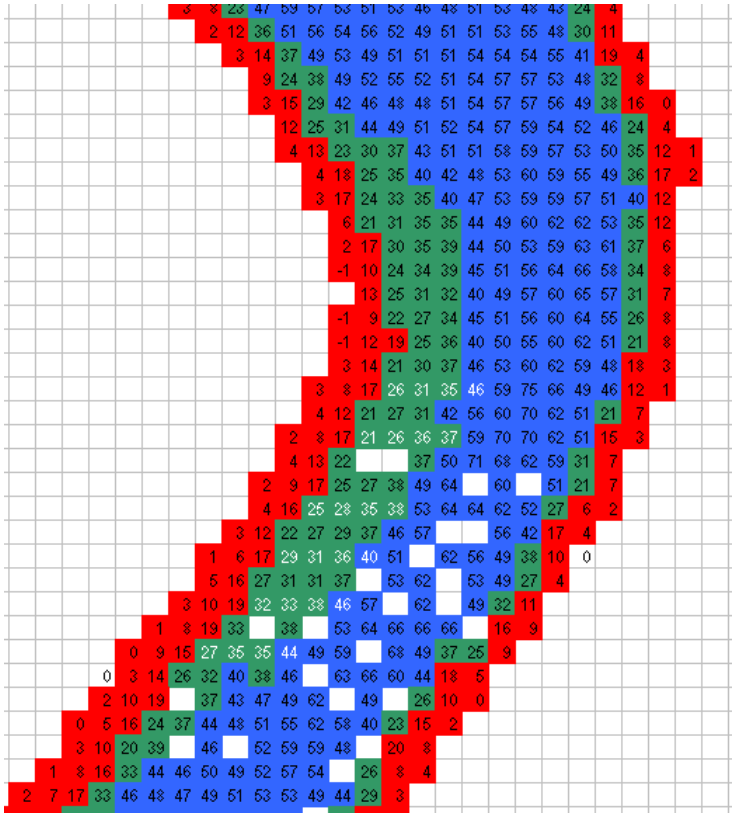

Figure B-2. Sample Bathymetric Spreadsheet Output for Tacoma Narrows

Interpolation in Soundings-Sparse Regions

For some older hydrographic surveys, soundings data are quite widely spaced and grid sizes would need to be rather large (>100m) to avoid generating a map with too many empty grid elements. Such representation of sparse data tends to overstate channel width and cross-section. An additional macro was written to "fill-in" the gaps resulting from using finer grids. The macro sweeps through the digital map, and when it encounters an empty grid, fills it in by taking an average of the surrounding grid points. The sweep repeats itself, eventually filling in the entire grid. On each sweep, grid elements that have been calculated by averaging their neighbors are re-averaged. Sweeps continue until the change in total depth for the entire grid (residual) falls below a defined limit.

This interpolation procedure assumes that bathymetry changes gradually between two grid elements of known depth, and that there are no local high or low points in the empty grid spaces. Navigational charts were consulted to verify that significant bathymetric features were not missed and that the resulting interpolated map accurately represented the channel.

The data available for Tacoma Narrows were sparse, and significant interpolation was needed to establish a suitably fine grid, as shown below.

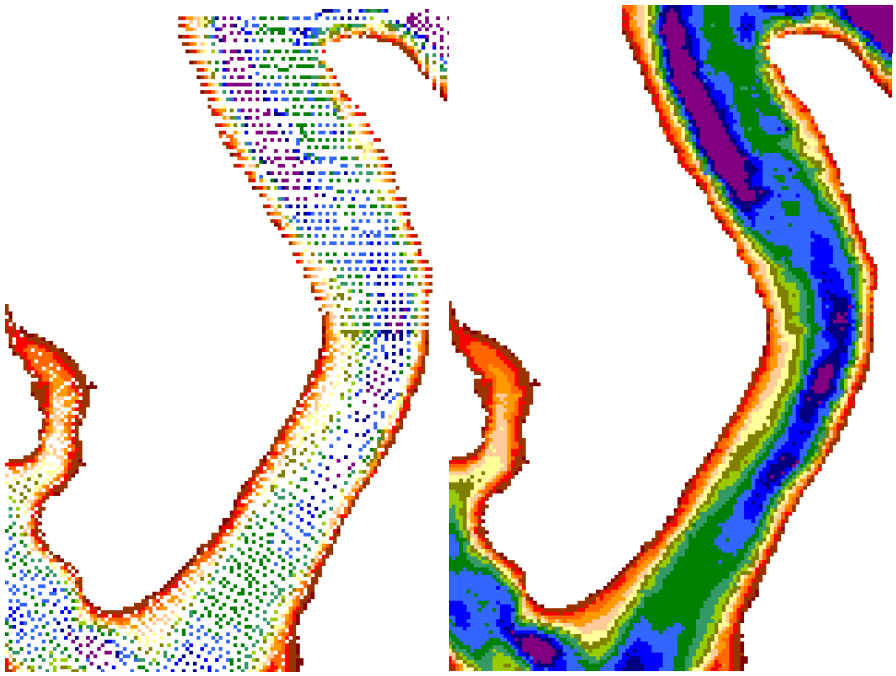

Figure B-3. Tacoma Narrows Digital Bathymetry Interpolation

By comparison, soundings data for Knik Arm were dense, and little interpolation was needed.

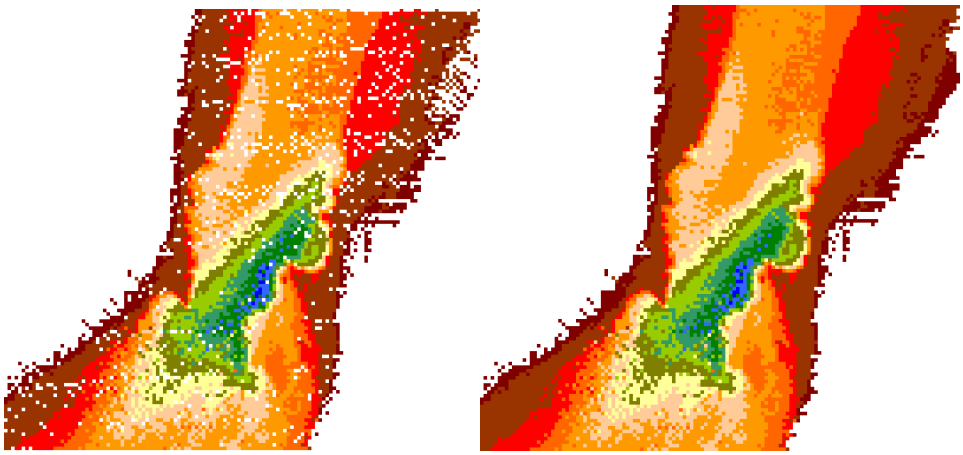

Figure B-4. Knik Arm Digital Bathymetry Interpolation